EFFECT OF TEMPERATURES ON SHEAR STRENGTH

OF FRACTURES IN GRANITE

Pakpoom Naphudsa

A Thesis Submitted in Partial Fulfillment of the Requirements for the

Degree of Master of Engineering in Geotechnology

Suranaree University of Technology

Academic Year 2013

ผลกระทบของอุณหภูมิต่อกำลังเฉือนของรอยแตกในหินแกรนิต

นายภาคภูมิ นาพุดซา

วิทยานิพนธ์นี้เป็นส่วนหนึ่งของการศึกษาตามหลักสูตรปริญญาวิศวกรรมศาสตรมหาบัณฑิต
สาขาวิชาเทคโนโลยีธรณี
มหาวิทยาลัยเทคโนโลยีสุรนารี
ปีการศึกษา 2556

EFFECT OF TEMPERATURES ON SHEAR STRENGTH OF FRACTURES IN GRANITE

Suranaree University of Technology has approved this thesis submitted in partial fulfillment of the requirements for a Master's Degree.

Thesis Examining Committee

_____

(Dr. Prachya Tepnarong)

Chairperson

_____

(Prof. Dr. Kittitep Fuenkajorn)

Member (Thesis Advisor)

_____

(Dr. Decho Phueakphum)

Member

_____

(Prof. Dr. Sukit Limpijumnong)

Vice Rector for Academic Affairs

and Innovation

_____

(Assoc. Prof. Flt. Lt. Dr. Kontorn Chamniprasart)

Dean of Institute of Engineering

ภาคภูมิ นาพุดซา : ผลกระทบของอุณหภูมิต่อกำลังเฉือนของรอยแตกในหินแกรนิต
(EFFECT OF TEMPERATURES ON SHEAR STRENGTH OF FRACTURES IN
GRANITE) อาจารย์ที่ปรึกษา : ศาสตราจารย์ ดร.กิตติเทพ เฟื่องขจร, 60 หน้า.

วัตถุประสงค์ของการศึกษาคือเพื่อหากำลังเฉือนของรอยแตกในตัวอย่างหินแกรนิตภายใต้
อุณหภูมิสูง การทดสอบค่ากำลังเฉือนในสามแกนได้ใช้โครงกดทดสอบในสามแกน โดยหา
ผลกระทบของอุณหภูมิต่อรอยแตกผิวขรุขระและรอยแตกผิวเรียบ โครงกดทดสอบในสามแกน
สามารถให้ความเค้นล้อมรอบคงที่ในขณะที่เพิ่มความเค้นในแนวแกน ในการทดสอบได้ใช้อัตรา
การกดเท่ากับ 1 เมกะปาสคาลต่อวินาที และหยุดทดสอบเมื่อระยะการเคลื่อนตัวในแนวเฉือนเท่ากับ
2   มิลลิเมตร ตัวอย่างที่ใช้ในการทดสอบเตรียมมาจากหินแกรนิตชุดตากโดยมีขนาดเท่ากับ
5.0×5.0×8.7 ลูกบาศก์เซนติเมตร พื้นที่รอยแตกมีค่าเท่ากับ 5×10 ตารางเซนติเมตร ความเค้นตั้งฉาก
บนรอยแตกทำมุม 60 องศา กับความเค้นในแนวแกน (ความเค้นหลัก) โดยทำการทดสอบภายใต้
อุณหภูมิที่ 303 เคลวิน (อุณหภูมิห้อง), 373, 573 และ 773 เคลวิน และผันแปรความเค้นล้อมรอบที่
1, 3, 7 12 และ 18 เมกะปาสคาล อุณหภูมิสูงถูกเพิ่มโดยการใช้ขดลวดให้ความร้อนโดยมีชุดความ
คุมอุณหภูมิด้วย   ผลการทดสอบของรอยแตกผิวขรุขระระบุว่าค่ากำลังเฉือนลดลงเมื่ออุณหภูมิ
เพิ่มขึ้น เกณฑ์การแตกของ Barton สามารถอธิบายกำลังเฉือนภายใต้อุณหภูมิสูงได้ดี กำลังเฉือน
ของรอยแตกผิวเรียบมีแนวโน้มเพิ่มขึ้นเมื่ออุณหภูมิสูงกว่า 373 เคลวิน ผลการทดสอบเหล่านี้ช่วย
ให้ปรับปรุงและพัฒนาความเข้าใจการต้านทานของรอยแตกในหินแกรนิตภายใต้ความเค้นสามแกน
และอุณหภูมิสูง

สาขาวิชา เทคโนโลยีธรณี   ลายมือชื่อนักศึกษา_____
ปีการศึกษา 2556   ลายมือชื่ออาจารย์ที่ปรึกษา_____

PAKPOOM NAPHUDSA : EFFECT OF TEMPERATURES ON SHEAR

STRENGTH OF FRACTURES IN GRANITE. THESIS ADVISOR : PROF.

KITTITEP FUENKAJORN, Ph.D., P.E., 60 PP

FRACTURE/GRANITE/SHEAR/COHESION/FRICTION ANGLE

The objective of this study is to experimentally determine the shear

strength of fractures in granite under elevated temperatures. The triaxial shear test

is performed using a polyaxial load frame. The effects of temperature on the peak

shear strengths of tension-induced fractures and smooth saw-cut surfaces are

determined. The polyaxial load frame applies confining (lateral) stresses while the

axis stress is increased. The axial load is applied at the rate of 1 MPa/s until a

total displacement of 2 mm is reached. The specimens are prepared from Tak

granite with nominal dimensions of $5.0 \times 5.0 \times 8.7$ cm^3 with the fracture area of

5.0×10.0 cm^2. The normal of fracture plane makes an angle of 60° with the axial

(major principal) stress. The testing is subjected to constant temperature ranging

from 303 (ambient temperature), 373, 573 to 773 Kelvin with lateral stress at 1, 3,

7, 12 and 18 MPa. The elevated temperatures are applied by using heating steel

coils with temperature regulator. For tension-induced fracture, the results indicate

that the shear strength decreases with increasing temperatures. Barton's criterion

can best describe the shear strength under elevated temperatures. The shear

strength of saw-cut surfaces tends to increase with temperature particularly above

373 Kelvin. These findings improve and develop the understanding of the

shearing resistance of fractures in granite under the triaxial stresses and elevated temperatures.

School of Geotechnology   Student's Signature_____

Academic Year 2013   Advisor's Signature_____

ACKNOWLEDGEMENTS

Pakpoom Naphudsa

TABLE OF CONTENTS

TABLE OF CONTENTS (Continued)

TABLE OF CONTENTS (Continued)

LIST OF TABLES

LIST OF FIGURES

LIST OF FIGURES (Continued)

LIST OF FIGURES (Continued)

SYMBOLS AND ABBREVIATIONS

a	=	Inside radius
c, S_o	=	Cohesion
d_1	=	Displacement of fracture in direction of σ_1
d_3	=	Displacement of fracture in direction of σ_3
d_n	=	Normal displacement
d_s	=	Shear displacement
E	=	Elastic modulus
JRC	=	Joint roughness coefficient
P_1	=	Vertical stress
P_2	=	lateral stress
r	=	Variable radius
α	=	Empirical constant
β	=	Angle between direction of σ_1 and σ_3
ϕ	=	Friction angle
ϕ_b	=	Basic friction angle
λ	=	Empirical constant
σ_1	=	Maximum principal stress
σ_2	=	Intermediate principal stress
σ_3	=	Minimum pressures
σ_n	=	Normal stress

SYMBOLS AND ABBREVIATIONS (Continued)

σ_r	=	Radial stress
σ_θ	=	Tangential stress
σ_c	=	Uniaxial compressive strength
σ_j, JCS	=	Joint wall compressive strength
τ	=	Shear stress
$\tau_{r\phi}$	=	shear stress around tunnel
τ_{xx}	=	Stress in direction x
τ_{xy}	=	Shear in direction x-y
τ_{yy}	=	Stress in direction y
μ	=	Coefficient friction
ω	=	Empirical constant
χ	=	Empirical constant
ξ	=	Empirical constant

CHAPTER I

INTRODUCTION

1.1   Rationale and background

Temperature is one of the main factors influencing the mechanical behavior of rock (Stesky, 1975; Dwivedi et al., 2008). Several researchers (Blanpied et al., 1995; Ohnaka, 1995; Kawamoto and Shimamoto., 1998; Odedra et al., 2001) have studied the effects of temperature on the rock physical and mechanical properties. The results indicate that temperature influences the friction angle, cohesion and shear strength of rocks. Tisa and Kovari (1984) have experimentally determined the frictional resistance of rock fractures under confinements. The cylindrical rock core containing an inclined fracture or weakness plane can be axially loaded under triaxial pressure. The normal stress at which the shear strengths are measured can be controlled by the applied axial stress and confining pressure (Lane and Heck, 1964; Rosso, 1976). The test provides the shear strengths of rock fractures under uniform lateral confining stresses ($\sigma_1 \neq \sigma_2 = \sigma_3$). The thermal effects on shearing resistance of fractures under confinements however have never been assessed.

The advantages of the deep hole injection in granite technology are that the rock at depth usually has less fracture, low permeability and resistant high temperature that may come from decay of radioactive waste. It is necessary to study the fracture stability in granite mass under elevated temperatures for the assessing

safety of the repository for heat generating nuclear waste in a deep geological rock formation.

1.2   Research objectives

The objective of this study is to experimentally determine the shear strengths of fractures in granite under elevated temperatures. The triaxial shear test will be performed using a polyaxial load frame. The effects of temperature on the peak shear strengths of tension-induced fractures and saw-cut surfaces are determined. Empirical equations will be derived to represent the shear strength of fractures as a function of temperature.

1.3   Research methodology

The research methodology shown in Figure 1.1 comprises 5 steps; including literature review, sample preparation, laboratory testing, development of mathematical relations, discussions conclusions and thesis writing.

1.3.1   Literature review

Literature review is carried out to study the previous researches on dependent the effect of the temperature on the shear strength of granite under triaxial stress and reposition of nuclear waste technology. The sources of information are from text books, journals, technical reports and conference papers. A summary of the literature review is given in the thesis.

1.3.2   Sample preparation

The granite samples used in this research is Tak granite. Sample preparation is carried out in the laboratory at the Suranaree University of Technology.

The rock samples are cut to obtain rectangular block specimens with nominal dimensions $5.0 \times 5.0 \times 8.7$ cm^3. The fractures are artificially made in the laboratory by tension-induced method and cutting machine. The asperity amplitudes on the fracture planes are used to estimate the joint roughness coefficients (JRC) of each fracture based on Barton's chart (Barton, 1982).

1.3.3 Laboratory testing

The triaxial shear tests under elevated temperatures are performed to determine the shear strength and to develop sliding criteria of the granite fractures by using the polyaxial load frame. The testing is subjected to nominal temperatures ranging from 303 (ambient temperature), 373, 573 to 773 Kelvin and each temperature is tested at confining stresses at 1, 3, 7, 12 and 18 MPa, respectively. The confining stresses are constant while the shear is increased until peak shear stresses are reached.

1.3.4 Mathematical relations

Results from laboratory measurements are presented in terms of major principal stresses (σ_1) corresponding to the peak shear strength (τ) as a function of normal stress (σ_n) for various temperatures. The testing results are used to develop relations between temperatures and friction angle (ϕ) and cohesion (c) to determine a new failure criterion for joint shear strength under elevated temperatures. A strength criterion that can incorporate the temperature is derived.

1.3.5 Discussions, conclusions and thesis writing

Discussions are made to analyze the impacts of the temperature and determine a new failure criterion for joint shear strength under elevated temperatures by polyaxial load frame. All research activities, methods and results are documented
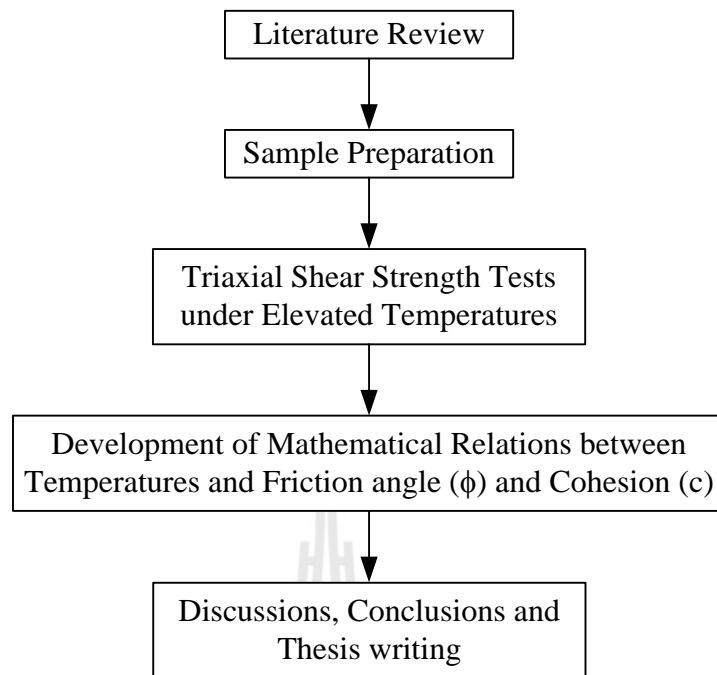
Figure 1.1 Research methodology

and complied in the thesis. The research or finding is published in the conference proceedings or journals.

1.4 Scope and limitations

The scope and limitations of the research include as follows:

1. Laboratory experiments are conducted on specimens from Tak granite.

2. All tested tension-induced fractures are artificially made in the laboratory by tension-inducing methods.

3. All tested saw-cut surfaces are artificially made in the laboratory by cutting machine.

4. The specimens are prepared with nominal dimensions of $5.0 \times 5.0 \times 8.7$ cm^3 with the fracture area of 5.0×10.0 cm^2.

5. The shear testing on fractures are made under confining stresses varies from 1, 3, 7, 12 and 18 MPa.

6. The nominal temperatures vary from 303, 373, 573 and 773 Kelvin.

7. All tests are performed using a polyaxial load frame.

8. A new shear strength criterion is derived from the test results.

1.5   Thesis contents

Chapter I introduces the thesis by briefly describing the background of problems and significance of the study. The research objectives, methodology, scope and limitations are identified. **Chapter II** summarizes the results of the literature review. **Chapter III** describes the sample preparation. **Chapter IV** proposes the laboratory experiment and presents the results obtained from the laboratory testing. **Chapter V** describes mathematical equations to determine the temperatures effect on shear strength of fractures rock. **Chapter VI** discusses and concludes the research results, and provides recommendations for future research studies.

CHAPTER II

LITERATURE REVIEW

2.1   Introduction

This chapter summarizes the results of literature review carried out to improve an understanding of the effects of temperatures on the shear strength of rock joints. The topics reviewed here include effects of temperature on rock fractures, and rock strength, shear strength calculation, and deep hole injection technology.

2.2   Literature review

2.2.1   Effects of temperature on rock fractures

Mitchell et al. (2013) state that temperature is believed to have an important control on frictional properties of rocks, yet the amount of experimental observations of time-dependent rock friction at high temperatures is rather limited. They investigated frictional healing of Westerly granite in a series of slide-hold-slide experiments using a direct shear apparatus at ambient temperatures between 20°C and 550°C. They observe that at room temperature coefficient of friction increases in proportion to the logarithm of hold time at a rate consistent with findings of previous studies. For a given hold time, the coefficient of friction linearly increases with temperature, but temperature has little effect on the rate of change in static friction with hold time. They used a numerical model to investigate whether time-dependent increases in real contact area between rough surfaces could account for the observed

frictional healing. The model incorporates fractal geometry and temperature-dependent viscoelasoplastic rheology. They explored several candidate rheologies that have been proposed for steady state creep of rocks at high stresses and temperatures. None of the tested laws could provide an agreement between the observed and modeled healing behavior given material properties reported in the bulk creep experiments. An acceptable fit to the experimental data could be achieved with modified parameters. In particular, for the power-law rheology to provide a reasonable fit to the data, the stress exponent needs to be greater than 40. Alternative mechanisms include time-dependent gouge compaction and increases in bond strength between contacting asperities.

Stesky (1978) studies the mechanical properties of faulted and jointed rock under pressure and temperature and in the presence of water. At low effective confining pressures (below about 1 kilobar), the friction strength is quite variable and depends on the frictional resistance between gouge particles or asperities and on the dilatancy of the fault. At higher pressures the friction strength is nearly independent of mineralogy, temperature, and rate, at least for rocks whose friction strength is less than the failure strength. Water tends to slightly weaken the fault. The type of sliding motion, whether stick-slip or stable sliding, is much more affected by environmental and mineralogical factors. In general, stick-slip is dominant at high pressures and low temperatures, in the presence of strong minerals such as quartz and feldspar, in the absence of gouge, for lower surface roughness, and perhaps in the presence of water. The microscopic deformation mechanisms are poorly understood. At low temperatures, cataclasis dominates in rocks containing mostly quartz or feldspar, and plastic deformation in rocks containing mostly calcite or platy silicates. At high of

most minerals deform plastically, producing a greater temperature and rate-dependence of the friction strength. Glass has been found in some sliding surfaces in sandstone.

Stesky et al. (1974) study the frictional behavior of seven low-porosity silicate rocks at temperatures of 700°C and pressures from 2.5 to 6 kbar. For all rocks except one, peridotite, stick-slip occurred at low temperature and gave way to stable sliding at some high temperature, different for each rock. These differences could be related to the presence or absence of minerals such as amphibole, mica, or serpentine. Up to some temperature, depending on rock type, the friction stress was relatively unaffected by temperature. The shear stress decreases at higher temperature, and in some cases such decrease is related to the coincidence of fracture and friction strength. While somewhat dependent on rock type, the friction stress for the seven rocks studied was about the same, within 10-15%. Up to 265°C, water had little effect on the frictional behavior of faulted granite at 3 kbar effective pressure. The frictional stresses measured in the laboratory were significantly higher than estimated for natural faults. This difference could be accounted for by high pore pressure or weak alteration materials in the natural fault zone.

Kawamoto and Shimamoto (1998) study shearing experiments on mixed halite-calcite layers to understand the behavior of bimineralic fault zones, using a high-temperature biaxial testing machine at rate of 0.3 µm/s and shear strains to about 30. Temperature was increased to 700°C in linear proportion to normal stress, with the experimental geotherm of about 22°C/MPa. The experimental data clearly demonstrate that the effect of mineral composition on the frictional strength at the temperature of 600°C and normal stress of about 24-27 MPa. The behavior of pure

halite shear zones is fully plastic under these conditions that shear resistance is nearly independent of normal stress. No strength peak is observed in the 75% halite experiment. The 2% halite specimen displays stick-slip soon after the peak friction is exceeded, the specimens containing more than 5% halite show only stable slip throughout the experiments.

Ohnaka (1995) evaluates quantitative effect of the normal stress and temperature on failure strength in brittle-plastic transition regime of Westerly granite by the published data. The result indicates that the effect of temperature is insignificant below 300°C for dry granite, suggesting that dry granite in this temperature range is in the brittle regime. Above 300°C, the temperature effect is greater. This may be related to development of localized plastic deformation in the shear failure zone. Westerly granite above 500°C may be ascribed to quartz plasticity (as well as biotite plasticity), since it has been reported that feldspar minerals do not deform plasticity at the experimental conditions.

Lockner et al. (1986) study the deformation on saw-cut granite surface inclined 30° to the sample axes. Sample diameters and lengths were 19.05 and 37.6 mm respectively, all samples were pre-dried at 270°C and 250 MPa of confining pressure for a minimum 1 hour. The sample was placed in a pressure vessel. Sample were deformed at a constant confining pressure of 250 MPa and temperatures of 22 to 845°C. The velocity dependent of the steady-state coefficient of friction was determined by comparing sliding strengths at different sliding rates. The results experimental have plotted axial stress as a function of temperature at 250 MPa of confining pressure and measuring at 2.9 mm of total displacement. Gouge strength

has increased approximately 15% at the highest temperatures. The relationship between axial stresses and temperatures is represented by:

$$\sigma_1 = 938 + 0.16T(C) \quad (MPa) \tag{2.1}$$

Parthasarathi et al. (2013) test to wear AISI type 316L(N) austenitic stainless steel at room temperature (25C), 100°C, 150°C, 250°C, 350°C, 450°C and 550°C respectively and study surface roughness by using Talysurf CLI 1000 surface profilometer. The surface profiles are analyzed using Talymap Platinum software version 4.1. The material softens with increase in temperature thereby resulting in increase in wear. Elastic modulus of AISI 316 L(N) decreases by about 23% when temperature is increased from room temperature to 550°C. The width of the wear track and frictional force too increased with increase in test temperature. The roughness surface may from nucleation sites for cracks or corrosion. Increase in frictional force would lead to more material loss during sliding wear.

Engelder (1976) studies the effect of scratch hardness on frictional wear and stick-slip of westerly granite and Cheshire quartzite with studying the mechanism of stick-slip, 1.2 cm diameter by 2.5 cm long cylinder specimens were slide in compression on surface inclined at 35° to the cylindrical axis. Experimental confining pressures on the dry samples were between 0.1 and 2.9 kb with an average sliding displacement rate 10^{-3} cm/sec. The scratch hardness of minerals on sliding surface affects the frictional properties of rocks. Highly polished quartz surfaces (Cheshire Quartzite) do not stick-slip below 2.5 kb confining pressure whereas highly polished quartz-feldspar surfaces (Westerly Granite) stick-slip at confining pressure

down to 0.3 kb. Because frictional wear seems to be necessary for stick-slip on highly

polished quartz surfaces, stick-slip will occur at confining pressures below 2.5 kb only

in the presence of minerals with scratch hardness than quartz and its greater

susceptibility to wear promotes stick-slip of Westerly granite at confining pressures

where Cheshire quartzite slides stably.

2.2.2 Effects of temperature on rock strength

Araújo et al. (1997) investigate the mechanical properties of reservoir

rocks obtained in laboratory at room temperature. The investigation was based on

triaxial tests performed by a servo-controlled system on samples of friable sandstone

cored from a reservoir in the Potigure Basin, Northwastern Brazil. The samples were

tested at 24°C, 80°C and 150°C with confining pressure varying from 2.5 MPa to 20

MPa. The resulting values for bulk compressibility indicate a significant decrease

with the temperature increasing from 24°C to 150°C. Figure 2.1 presents the

regression lines in the plane σ_1-σ_3, for the temperature 24°C and 150°C.
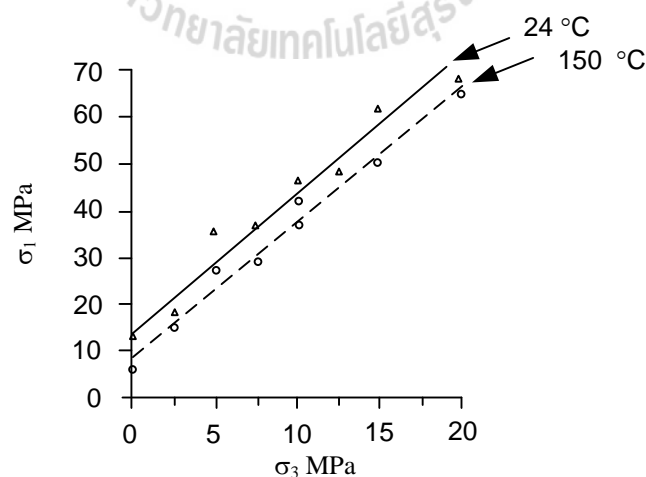
Figure 2.1 Failure limits from multiple failure state tests on sandstones from Acu

formation (Araujo et al., 1997).

Results show an average reduction of about 18% in the compressive strength for an increase of temperature from 24°C to 150°C.

Xu et al. (2009) state that the effect of temperature on mechanical characteristics and behaviors of granite was analyzed by using experiments as scanning electron microscope (SEM), X-ray diffraction and acoustic emission (AE) and the micromechanism of brittle-plastic transition of granite under high temperature was discussed as well. The rock specimens are 50 mm long, with diameters of 25 mm. The specimens of each were heated to the temperature ranging from 25 to 1300°C. The failure from of granite changes from abruptly brittle fracture to semi-brittle shear fracture gradually with the rise of temperature. The average of compressive strength and elastic modulus at different temperatures is seen as Table 2.1, which decreases with the rise of temperature.

Xu et al. (2008) propose the relationships between mechanical characteristics of rock and microcosmic mechanism at high temperatures which were investigated by MTS815, Based on a micropore structure analyzer and SEM, the changes in rock porosity and micro structural morphology of sample fractures and brittle-plastic characteristics under high temperatures were analyzed. The results are

Table 2.1 Average of compressive strength and elastic modulus at different

temperature (Xu et al., 2009).

Rock properties	Temperature(°C)							
	25	200	500	800	900	1000	1100	1200
Compressive strength σ_c (MPa)	191.9	135.96	151.9	185.22	89.94	71.61	77.98	36.09
Elastic modulus E (GPa)	38.57	28.68	31.25	25.11	11.02	8.39	6.61	2.87

as follows: 1) Mechanical characteristics do not show obvious variations before 800°C; strength decreases suddenly after 800°C and bearing capacity is almost lost at 1200°C, 2) Rock porosity increases with rising temperatures; the threshold temperature is about 800°C; at this temperature its effect is basically uniform with strength decreasing rapidly, and 3) The failure type of granite is a brittle tensile fracture at temperatures below 800°C which transforms into plasticity at temperatures higher than 800°C and crystal formation takes place at this time. Chemical reactions take place at 1200°C. Failure of granite under high temperature is a common result of thermal stress as indicated by an increase in the thermal expansion coefficient, transformation to crystal formation of minerals and structural chemical reactions.

Wai and Lo (1982) study the effects of temperature up to 350°C on the strength and deformation properties of rock. Particular attention was paid to the experimental procedure to avoid premature thermal cracking of the specimens. It was shown that the thermal-mechanical behavior varies with the rock type. For granitic gneiss, the deformation modulus increases slightly with temperature up to 120°C, then decreases at a rate of about 25% per 100°C. Poisson's ratio generally decreases with increasing temperature up to 250°C. The uniaxial compressive strength of granitic gneiss decreases with increasing temperature at a rate of the order of 30 MPa per 100°C. The deformation properties of the granitic gneiss are also dependent on the temperature history of the specimen. In contrast, both the deformation and strength behavior of the limestone appear to be insensitive to temperature change.

Zhao et al. (2012) perform triaxial compression system for rock testing under high temperature and high pressure. The performance and technological

innovations of a self-developed 20 MN rock triaxial test machine XPS-20MN for high temperature and high pressure are presented. The tests revealed the stress-strain characteristics of the coal specimens at high temperature, particularly the enhanced plastic features. Young's modulus decreases in a negative exponential function in regarding to the temperature. Test results revealing the thermal deformation and failure mode of the large-size granite specimens at high temperature and high pressure, and the changing of the thermodynamic parameters of the specimen, such as Young's modulus, with temperature, are also present as examples of test carried out using the testing machine.

2.2.3 Shear strength calculation

Jaeger et al. (2007) state that in order to derive the laws that govern the transformation of stress components under a rotation of the coordinate system, we again consider a small triangular element of rock, as in Figure 2.2. We arrive at the following
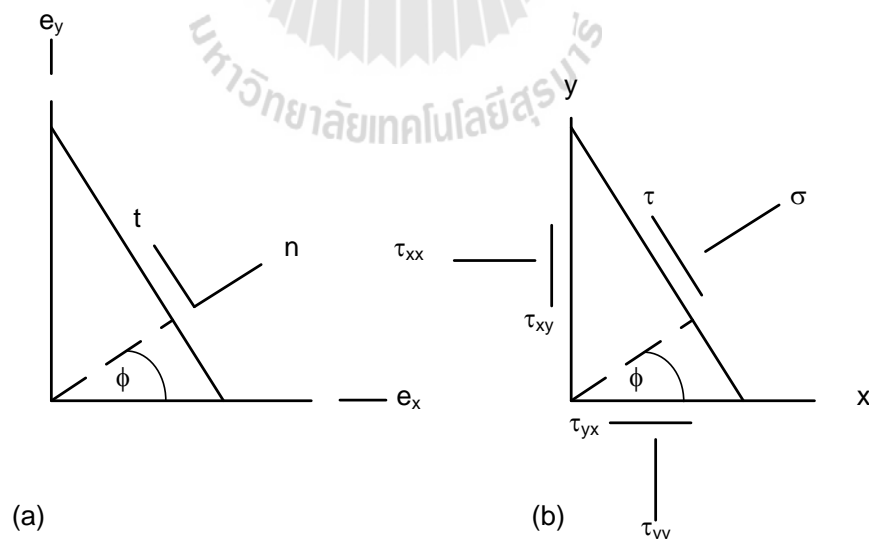
Figure 2.2 Small triangular slab of rock used to derive the stress transformation

(Jaeger et al., 2007)

equations for the normal and shear stresses acting on a plane whose outward unit normal vector is rotated counterclockwise from the x direction by an angle θ:

$$\sigma = \tfrac{1}{2}\,(\tau_{xx} + \tau_{yy}) + \tfrac{1}{2}\,(\tau_{xx} - \tau_{yy})\cos 2\theta + \tau_{xy}\sin 2\theta \qquad (2.2)$$

$$\tau = \tfrac{1}{2}\,(\tau_{yy} - \tau_{xx})\sin 2\theta + \tau_{xy}\cos 2\theta \qquad (2.3)$$

An interesting question to pose is whether or not there are planes on which the shear stress vanishes, and where the stress therefore has purely a normal component. The answer follows directly from setting $\tau = 0$, and solving for

$$\tan 2\theta = \frac{2\tau_{xy}}{\tau_{xx} - \tau_{yy}} \qquad (2.4)$$

A simple graphical construction popularized by Mohr (1914) can be used to represent the state of stress at a point. Recall that (1) and (2) give expressions for the normal stress and shear stress acting on a plane whose unit normal direction is rotated from the x direction by a counterclockwise angle θ. We replace τ_{xx} with σ_1, replace τ_{yy} with σ_2, replace τ_{xy} with 0 in the principal coordinate system, and interpret θ as the angle of counterclockwise rotation from the direction of the maximum principal stress. We thereby arrive at the following equations that give the normal and shear stresses on a plane whose outward unit normal vector is rotated by θ from the first principal direction:

$$\sigma = \frac{(\sigma_1 + \sigma_2)}{2} + \frac{(\sigma_1 - \sigma_2)}{2}\cos 2\theta \qquad (2.5)$$

$$\tau = \frac{(\sigma_1 - \sigma_2)}{2} \sin 2\theta \qquad (2.6)$$

The rock has a preexisting plane of weakness whose outward unit normal vector makes an angle β with the direction of the maximum principal stress, σ_1 (Figure 2.3). The criterion for slippage to occur along this plane is assumed to be

$$|\tau| = S_o + \mu\sigma \qquad (2.7)$$

where σ is the normal traction component acting along this plane and τ is the shear component. By (2.5) and (2.6), σ and τ are given by

$$\sigma = \tfrac{1}{2}(\sigma_1 + \sigma_2) + \tfrac{1}{2}(\sigma_1 - \sigma_2)\cos 2\beta \qquad (2.8)$$

$$\tau = -\tfrac{1}{2}(\sigma_1 - \sigma_2)\sin 2\beta \qquad (2.9)$$
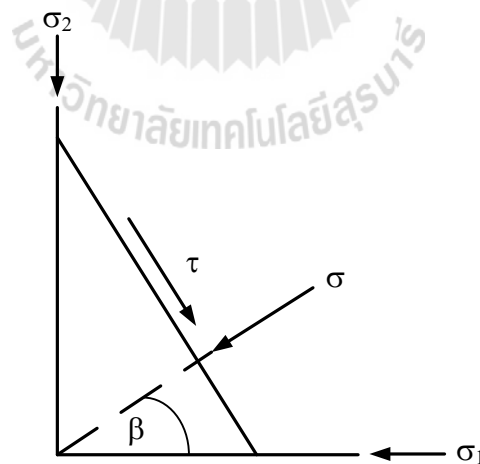
Figure 2.3 Plane of weakness with outward normal vector oriented at angle β to

the direction of maximum principal stress (Jaeger et al., 2007).

Barton and Choubey (1977) propose empirical non-linear equation for peak shear strength of rough unfilled joints based on the results of direct shear tests performed on a wide variety of model tension fractures. The proposed equation for peak shear strength is as follows, which is sensitive both to variable joint roughness and compressive strength for the rock or joint walls:

$$\tau = \sigma_n \tan [\phi_b + JRC \log_{10} (JCS/ \sigma_n)] \qquad (2.10)$$

where τ is shear strength at failure, σ_n is stress normal to the shear plane, ϕ_b is the basic friction angle on smooth planar sliding surface, JRC is the joint roughness coefficient and JCS is the joint wall compressive strength.

Hoek and Brown (1990) state that the stress distributions around a borehole (σ_r, σ_θ, $\tau_{r\theta}$) can be calculated by Kirsch solution:

$$\sigma_r = [(P_1 + P_2) / 2)][1 - (a^2/r^2)] + [(P_1 - P_2) / 2)][(1 - (4a^2/r^2)) +(3a^4/r^4)] \cos2\theta \quad (2.11)$$

$$\sigma_\theta = [(P_1 + P_2) / 2)][1 + (a^2/r^2)] - [(P_1 - P_2) / 2)][1 + (3a^4/r^4)] \cos2\theta \qquad (2.12)$$

$$\tau_{r\theta} = - [(P_1 + P_2) / 2)][(1 + (2a^2/r^2) - (3a^4/r^4)] \cos2\theta \qquad (2.13)$$

where σ_r is the stress in the direction of changing r, σ_θ is tangential stress, $\tau_{r\theta}$ is shear stress, P_1 is vertical stress, P_2 is lateral stress, a is inside radius of opening, r is variable radius and θ is the angle between vertical axis and radius.

2.2.4 Deep hole injection technology

Gibb et al. (2008) present waste actinides, including plutonium, present a long-term management problem and a serious security issue. Immobilisation in

mineral or ceramic waste forms for interim storage is a widely proposed first step. The safest, most secure geological disposal for Pu is in very deep boreholes and they propose that the key step to combination of these immobilisation and disposal concepts is encapsulation of the waste form in cylinders of recrystallized granite. They discuss the underpinning science, focusing on experimental work, and consider implementation. Finally, they present and discuss analyses of zircon, UO2 and Ce-doped cubic zirconia from high pressure and temperature experiments in granitic melts that demonstrate the viability of this solution and that actinides can be isolated from the environment for millions, maybe hundreds of millions, of years.

Gibb et al. (2008) states that deep (4–5 km) boreholes are emerging as a safe, secure, environmentally sound and potentially cost-effective option for disposal of high-level radioactive wastes, including plutonium. One reason this option has not been widely accepted for spent fuel is because stacking the containers in a borehole could create load stresses threatening their integrity with potential for releasing highly mobile radionuclides like 129I before the borehole is filled and sealed. This problem can be overcome by using novel high-density support matrices deployed as fine metal shot along with the containers. Temperature distributions in and around the disposal are modelled to show how decay heat from the fuel can melt the shot within weeks of disposal to give a dense liquid in which the containers are almost weightless. Finally, within a few decades, this liquid will cool and solidify, entombing the waste containers in a base metal sarcophagus sealed into the host rock.

Gibb (2003) proposes an alternative strategy for the disposal of spent nuclear fuel (SNF) and other forms of high-level waste (HLW) whereby the integrity of a mined and engineered repository for the bulk of the waste need be preserved for

only a few thousand years. This is achieved by separating the particularly problematic components, notably heat generating radionuclides (HGRs) and very long lived radionuclides (VLLRs) from the waste prior to disposal. Such a solution requires a satisfactory means of disposing of the relatively minor amounts of HGRs and VLLRs removed from the waste. This could be by high-temperature very deep disposal (HTVDD) in boreholes in the continental crust. However, the viability of HTVDD, and hence the key to the entire strategy, depends on whether sufficient melting of granite host rock can occur at suitable temperatures and whether the melt can be completely recrystallized. The high-temperature, high-pressure experiments reported here demonstrate that granite can be partially melted and completely recrystallized on a time scale of years, as opposed to millennia as widely believed. Furthermore, both can be achieved at temperatures and on a time scale appropriate to the disposal of packages of heat generating HLW. It is therefore concluded that the proposed strategy, which offers, environmental, safety and economic benefits, could be a viable option for a substantial proportion of HLWs.

Gibb (1999) states that safe disposal of radioactive waste, especially spent fuel, ex-military fissile materials and other forms of high-level waste (HLW), is one of the major challenges facing contemporary science. Currently, the internationally preferred solution is for geological disposal by interment in a mined and engineered, multi-barrier repository. Although this is often referred to as ``deep'' disposal, the depths involved are usually quite shallow in geological terms. A new scheme, currently under development, for the high-temperature disposal of concentrated HLW in very deep boreholes is outlined. Recent advances in the knowledge of continental crustal rocks and fluids at depths of several kilometres

suggest that much deeper disposal might offer a safer and environmentally more acceptable solution to the HLW problem. The new scheme seeks to capitalise on this potential while turning the problematical heat output of the waste to advantage. It appears to offer significant benefits over both mined repositories and earlier borehole scenarios, particularly in terms of safety.

Sundberg et al. (2009) state that Swedish Nuclear Fuel and Waste Management Company (SKB) are organized with the objective of sitting a deep geological repository for spent nuclear fuel. The spent fuel is encapsulated in 5 m long cylindrical copper/steel canisters with an outer diameter of 1.05 m. The canisters are deposited in vertical 8 m-deep, 1.75 m-diameter deposition holes excavated in the floor of horizontal deposition tunnels at 400–700 m depth in crystalline rock below ground surface. The insulation and protection, the canisters are surrounded by barrier of bentonite clay. The temperature peak occurs some 10 years after deposition and amounts to 87°C.

Witherspoon et al. (1979) investigate granite at Stripa, Sweden, for nuclear waste storage and state that the designing waste repositories must understand how such stresses are affected by the behavior of the fracture systems. The fractures affect the thermo-mechanical of the rock mass, but they provide the main pathways for radionuclides to migrate away from the repository.

CHAPTER III

SAMPLE PREPARATION

3.1 Introduction

Tak granite, Tak province, Thailand, has been selected for use as rock sample here primarily because it has low permeability, less fracture and resistant heating. Mahawat et al. (1990) give detailed description and origin of the Tak granite that Tak pluton cuts the Eastern and Western plutons, and has faulted and strongly sheared contacts with Lower Palaeozoic sediments. It is surrounded by extensive microgranite, porphyry and pegmatite dykes. The mineral compositions of the sample tested are plagioclase 16.2%, quartz 5.4%, K-fieldspar 5%, biotite 2.7%, hornblende 0.5%, Ore/Rest tr, groundmass 70% (Atherton et al.,1992).

3.2 Sample preparation

The specimens have been prepared to obtain rectangular blocks with nominal dimensions of $5 \times 10 \times 10$ cm^3. A line load is applied to obtain a tension-induced fracture across the granite block. The saw-cut surfaces have been prepared by cutting machine. Figure 3.1 shows some rock specimens after the fracture has been induced by tension-induced method and cut by cutting machine. The rock specimens are cut to obtain rectangular block specimens with nominal dimensions $5.0 \times 5.0 \times 8.7$ cm^3 as shown in Figure 3.2. The fracture surface has an area of 5×10 cm^2. The normal to the fracture plane makes an angle 60° with the axial of the specimens. All fractures are clean and well mated. The average density is 2.65 g/cc.

The asperity amplitudes on the fracture planes are measured from the laser-scanned profiles along the shear direction. The readings are made to the nearest 0.01 mm. The maximum amplitudes are used to estimate the joint roughness coefficients (JRC) of each fracture based on Barton's chart. The joint roughness coefficients are averaged as 12-16 (Table 3.1). Some scanned profiles are shown in Figure 3.3.

Table 3.1 Joint rough coefficients of the tension-induced fractures.

Sample No.	Maximum asperity amplitude (mm)	JRC
GRS_01	3.200	13
GRS_02	3.709	15
GRS_03	2.896	12
GRS_04	2.947	12
GRS_05	3.085	12
GRS_06	3.427	14
GRS_07	3.212	13
GRS_08	3.992	16
GRS_09	3.316	13
GRS_10	3.056	12
GRS_11	3.805	15
GRS_12	2.933	12
GRS_13	4.108	16
GRS_14	3.900	16
GRS_15	3.422	14
GRS_16	2.984	12
GRS_17	3.242	13
GRS_18	3.027	12
GRS_19	3.557	14
GRS_20	3.865	15

Table 3.1 Joint rough coefficients of the tension-induced fractures (continue).

Sample No.	Maximum asperity amplitude (mm)	JRC
GRS_21	3.495	14
GRS_22	4.012	16
GRS_23	2.877	12
GRS_24	2.879	12
GRS_25	3.283	13
GRS_26	3.846	15
GRS_27	4.106	16
GRS_28	3.836	15
GRS_29	3.749	15
GRS_30	3.543	14
GRS_31	2.981	12
GRS_32	3.883	16
GRS_33	3.772	15
GRS_34	3.510	14
GRS_35	2.879	12
GRS_36	3.104	12
GRS_37	3.668	15
GRS_38	3.464	14
GRS_39	3.002	12
GRS_40	3.105	12

a 10 cm

5 cm

b 10 cm

5 cm
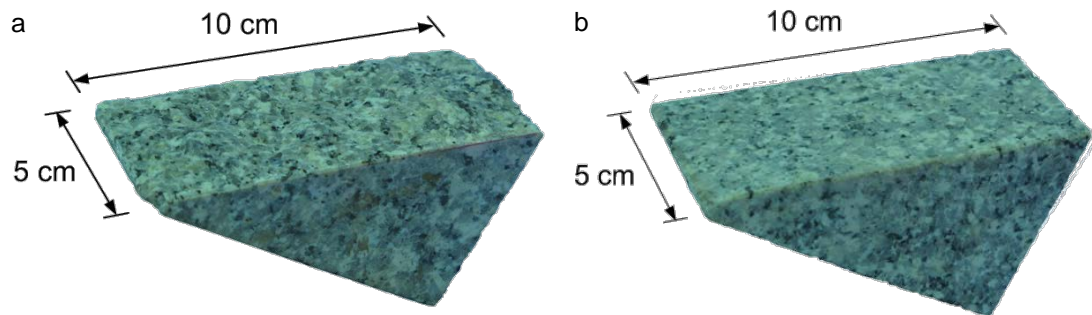
Figure 3.1 Fracture specimens are prepared by tension-induced (a) method and

cutting machine (b)

Line cut   Fracture

10 cm

5 cm   10 cm

GRS32-1

8.7 cm

GRS32-2

5 cm   5 cm
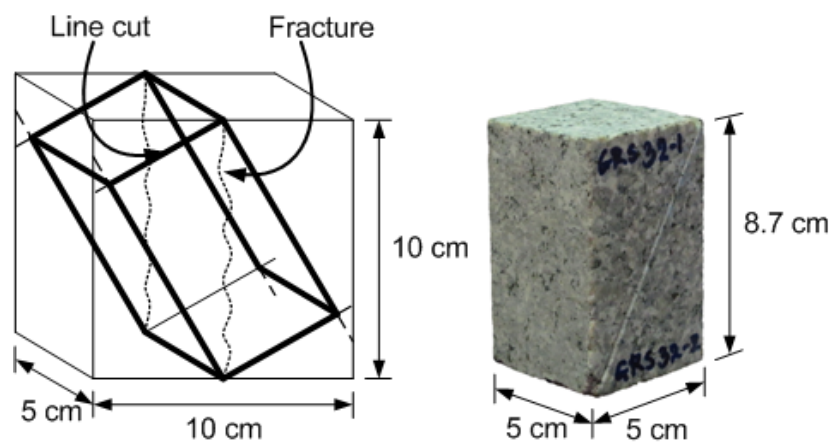
Figure 3.2 Rock samples cut to obtain rectangular block with nominal dimensions

$5.0 \times 5.0 \times 8.7$ cm^3.
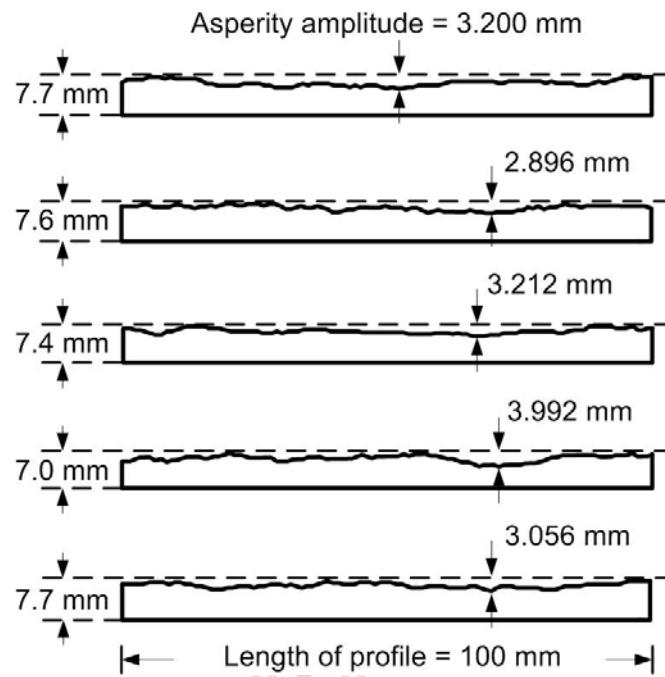
Figure 3.3 Examples of laser-scanned profiles to measure the maximum asperity

amplitude and to estimate the joint roughness coefficient.
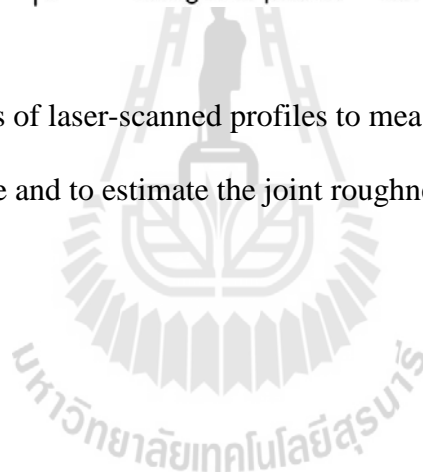
CHAPTER IV

LABORATORY TESTING

4.1 Introduction

The objective of the laboratory testing is to determine the effect of temperatures on shear strength of fractures. This chapter describes the method and calculation of the results and test results. It is composed of the shear strength on tension-induced fracture and saw-cut surface results under temperatures of 303, 373, 573 and 773 Kelvin, and confining pressures of 1, 3, 7, 12 and 18 MPa. The temperatures effect on shear strength results is studied to design deep disposal borehole.

4.2 Test apparatus

Steel platens with heater coil are the key component for this experiment. Its dimensions are shown in Figure 4.1. The heater coil is around the steel platen (Figure 4.2). Electric heating is through a resistor converts electrical energy into heat energy. Electric heating devices use Nichrome (Nickel-Chromium Alloy) wire supported by heat resistant. A thermostat (Figure 4.3) is a component of a control system which senses the temperature of a system so that the system's temperature is maintained near a desired setpoint. A heating element converts electricity into heat through the process of resistive. Electric current passing through the element encounters resistance, resulting in heating of the element. The thermostat apparatus is SHIMAX MAC5D-MCF-EN Series DIGITAL CONTROLLER. The digital controller have a

size of 48×48 mm and panel depth of 62-65 mm. Power supply is a 100-240V ± 10%AC on security surveillance system.   The accuracy is ± 0.3%FS + 1digit.   The thermocouple is type E1 that can measure the temperatures rang of 0-700°C.
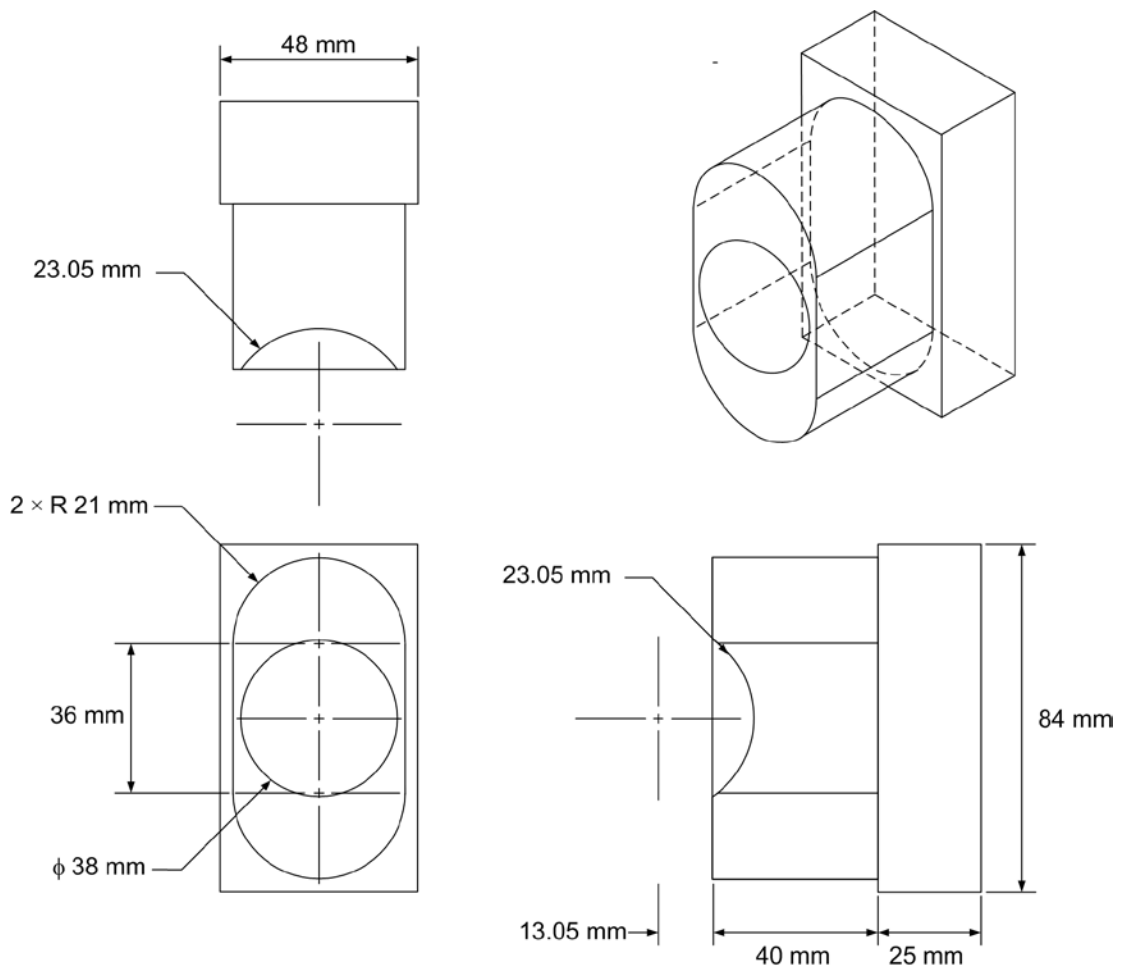
Figure 4.1 Steel platen dimensions.
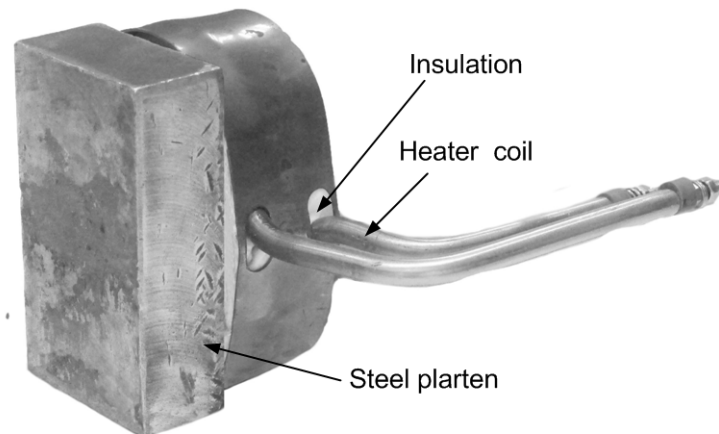
Figure 4.2 Heater coil entwine around steel platen.
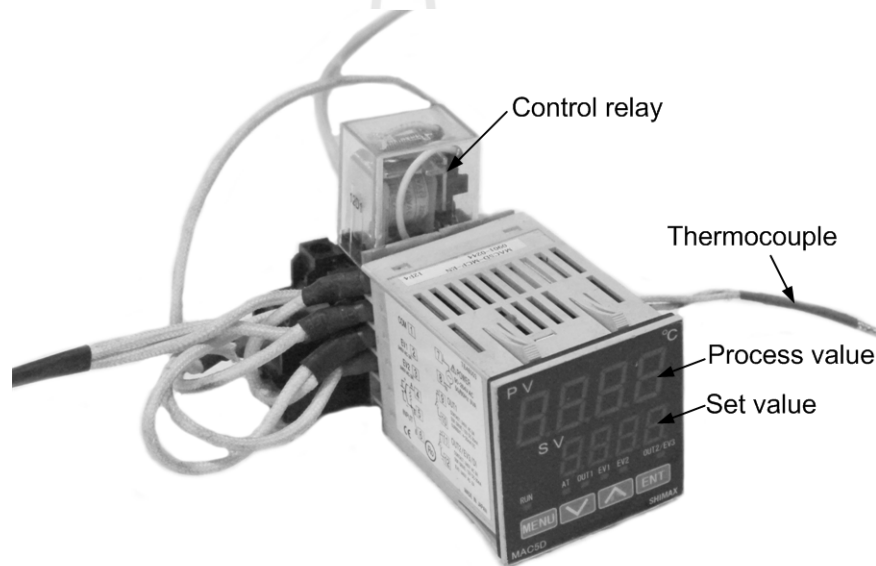
Figure 4.3 Thermostat.

4.3   Test method

The granite specimens are installed into a polyaxial load frame (Figure 4.4) (Fuenkajorn and Kenkhunthod, 2010) with steel platens. The platens are heated by heater coil for 2 hours before testing, at 373, 573 and 773 Kelvin (Figure 4.5). The temperature is measured and regulated by using thermocouple and thermostat. A digital temperature regulator is used to maintain constant temperature to the specimen. The changes of specimen temperatures between before and after testing are less than 5 Kelvin. Dead weights are placed on the two lower bars to obtain the pre-defined magnitude of the lateral stresses (confining pressures, σ_3) on the specimens. Simultaneously the axial stress (σ_1) is increased to the same value with lateral stresses to obtain the condition where both shear and normal stresses are zero on the fracture axial stress at a constant rate using the oil pump while lateral stresses are maintained constant. The specimen deformations in the three loading directions are monitored by dial indicator (dial gauge). The readings are recorded in every 8.4 kN of the axial load increment until the peak shear stress is reached. Figure 4.6 shows the directions of the applied stresses with respect to the fracture orientation. The test is terminated after the axial displacement of 10 mm is reached. The specimen is removed from the load frame. Post-test fracture is examined and photographed.
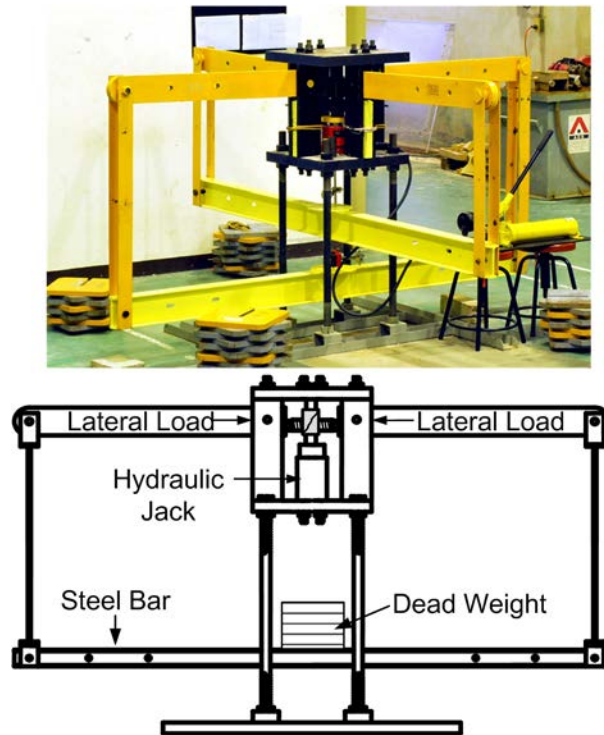
Figure 4.4 Polyaxial load frame (Fuenkajorn and Kenkhunthod, 2010).
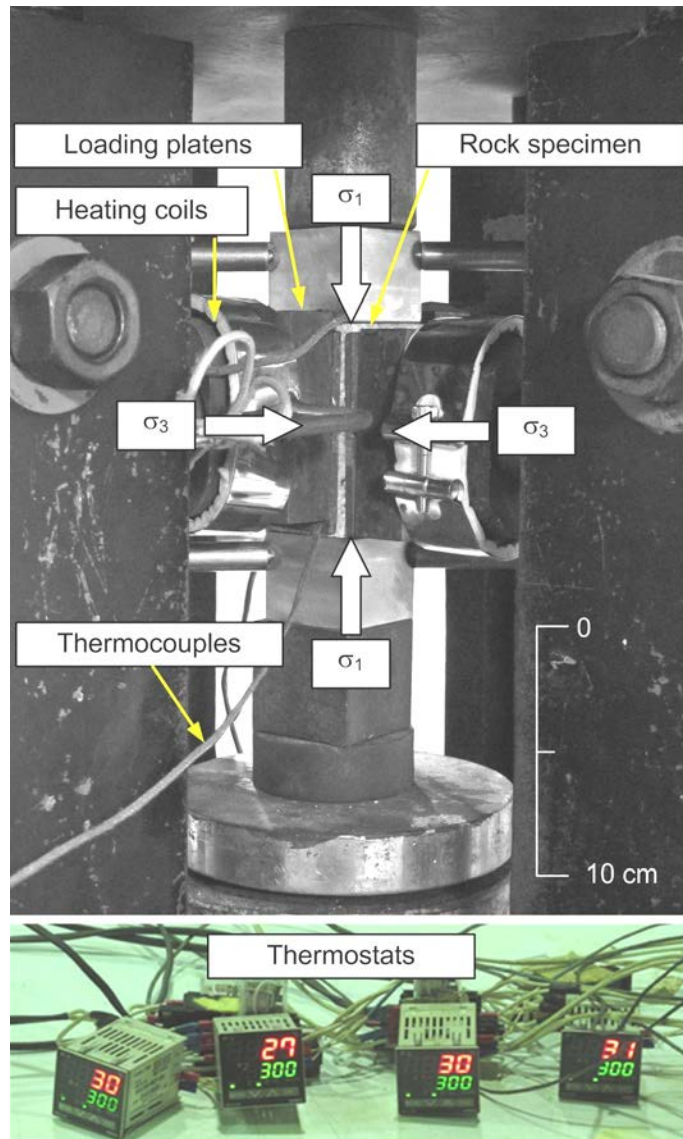
Figure 4.5   Temperatures measured and regulated by thermocouples and

thermostats.
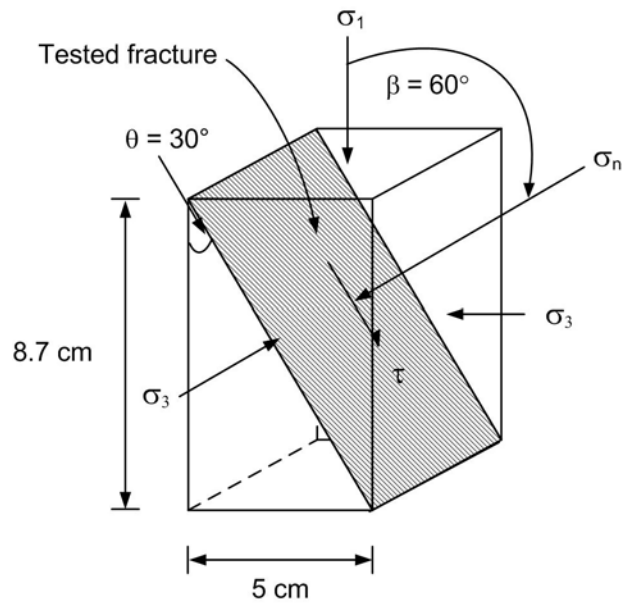
Figure 4.6 Directions of the applied stresses with respect to the fracture orientation.

4.4 Calculation of the results

The shear stress (τ) and its corresponding normal stress (σ_n) increase with σ_1, which can be determined as follows (Jaeger et al., 2007):

$$\tau = \frac{1}{2}(\sigma_1 - \sigma_3) \cdot \sin 2\beta \tag{4.1}$$

$$\sigma_n = \frac{1}{2}(\sigma_1 + \sigma_3) + \frac{1}{2}(\sigma_1 - \sigma_3) \cdot \cos 2\beta \tag{4.2}$$

where β is the angle between σ_1 and σ_n directions. For all specimens the angle β equals to 60 degrees. The relative shear and normal displacements (d_s and d_n) are calculated by:

$$d_s = \frac{1}{2}(d_1 - d_3) \cdot \sin 2\beta \qquad (4.3)$$

$$d_n = \frac{1}{2}(d_1 + d_3) + \frac{1}{2}(d_1 - d_3) \cdot \cos 2\beta \qquad (4.4)$$

where d_1 and d_3 are the relative displacements of the fracture monitored in the directions of σ_1 and σ_3 during the test, respectively.

4.5   Test results

4.5.1   Shear strength of tension-induced fractures

The peak shear strengths of the tension-induced fractures are determined under the temperatures of 303, 373, 573 and 773 Kelvin and confining stresses from 1, 3, 7, 12 to 18 MPa. Table 4.1 summarizes the shear strength results. The results indicate that the shear strength decreases with increasing temperature. Examples of the shear stress-displacement (τ-d_s) curves for specimens are shown in Figure 4.7. Non-linear behavior of the fracture is reflected as a curvature of the shear strength-normal stress diagram. Shear strengths are plotted as a function of normal stresses for various temperatures in Figure 4.8. Figure 4.9 shows the fracture dilation (normal displacement) as a function of the shear displacement monitored during the test. Post-test observations show that the sheared off areas for the fractures under higher temperatures tend to be larger than those tested under lower temperatures (Figure 4.10)

Table 4.1 Peak shear strengths of tension-induced fractures.

Temperatures, T (Kelvin)	Confining pressures, σ_3 (MPa)	Axial strengths, σ_1 (MPa)	Normal stresses, σ_n (MPa)	Shear strength, τ (MPa)
303	1	32.08	8.77	13.46
	3	84.44	23.36	35.26
	7	135.03	39.01	55.44
	12	167.67	50.92	67.41
	18	196.55	62.64	77.31
373	1	37.03	10.01	15.16
	3	72.62	20.4	30.14
	7	110.45	32.86	44.79
	12	141.45	44.37	56.06
	18	170.84	56.21	66.18
573	1	35.23	9.56	14.82
	3	60.75	17.44	25.01
	7	96.05	29.26	38.97
	12	125.09	40.27	48.97
	18	141.13	48.78	53.32
773	1	32.03	8.76	13.44
	3	47.96	14.24	19.47
	7	73.64	23.66	28.86
	12	96.22	33.06	36.47
	18	112.26	41.57	40.82
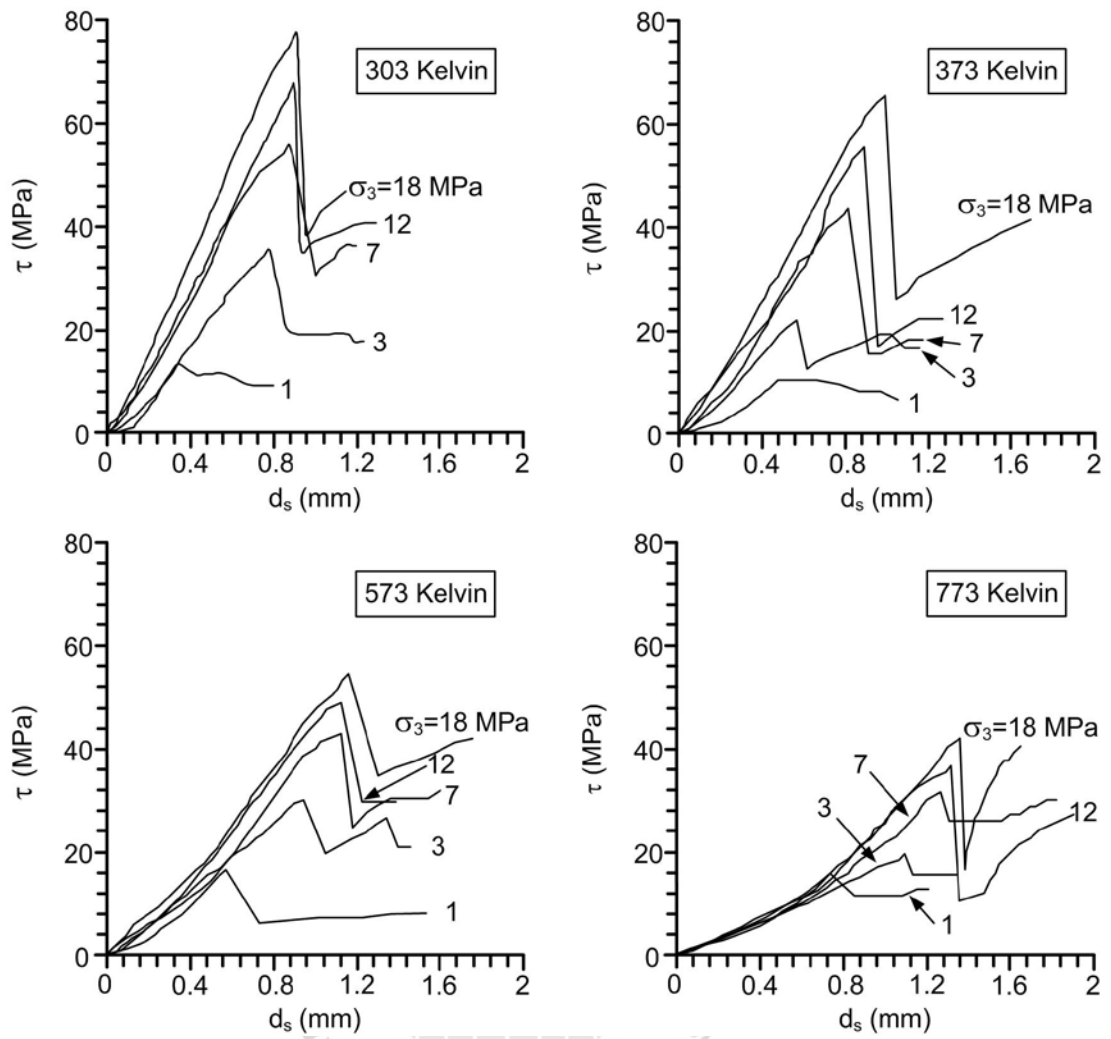
Figure 4.7   Shear stresses as a function of shear displacements of tension-induced
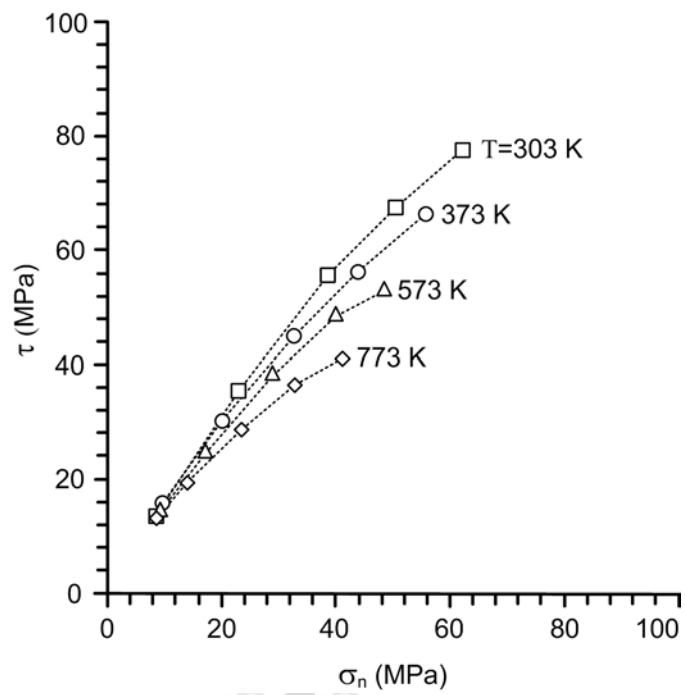
fractures.

Figure 4.8   Shear stresses as a function of normal stresses of tension-induced
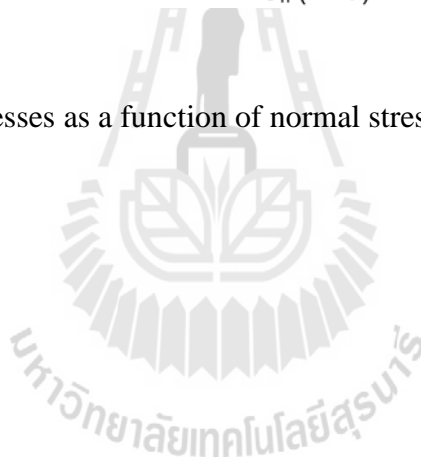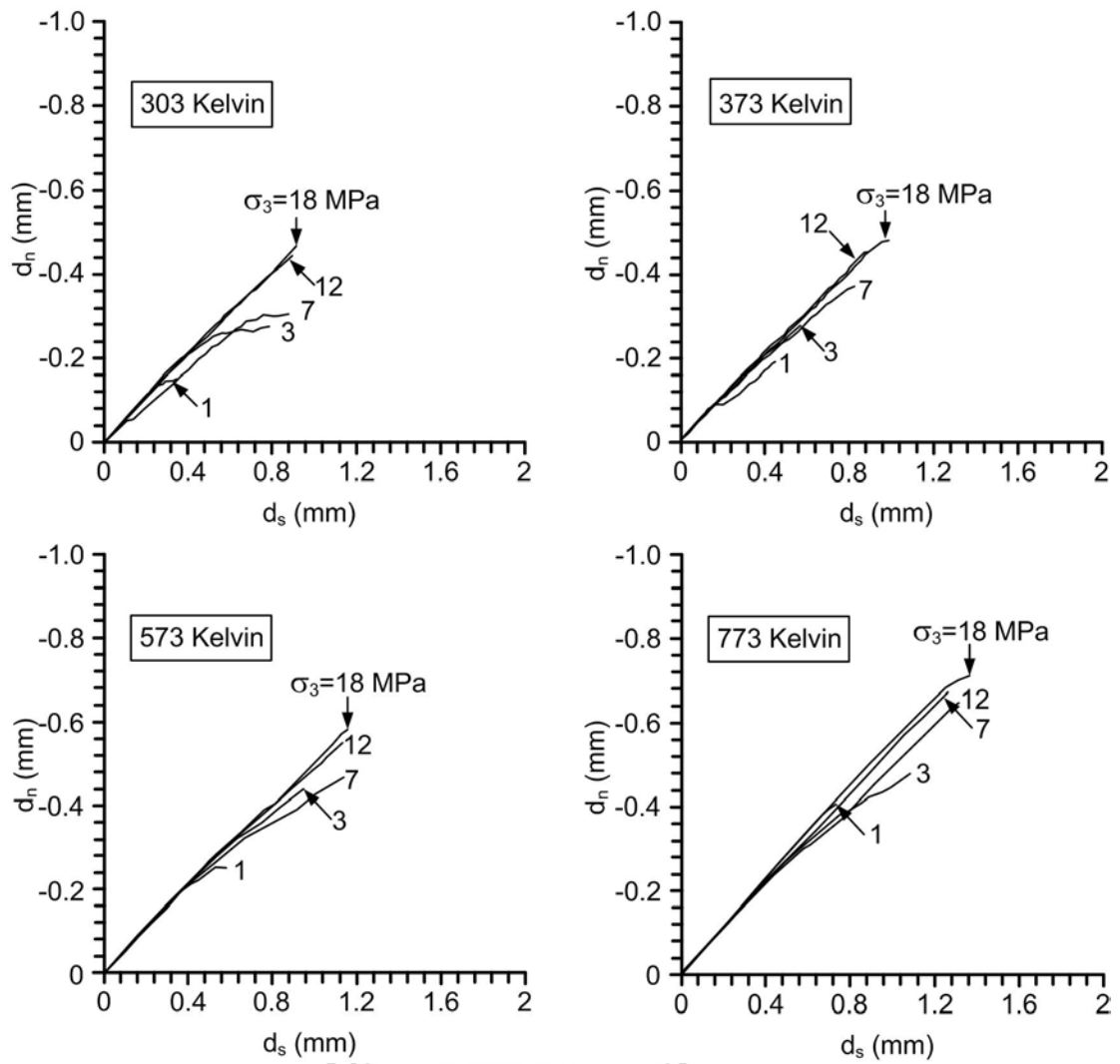
fractures.

Figure 4.9 Normal displacements as a function of the shear displacements of

tension-induced fractures.
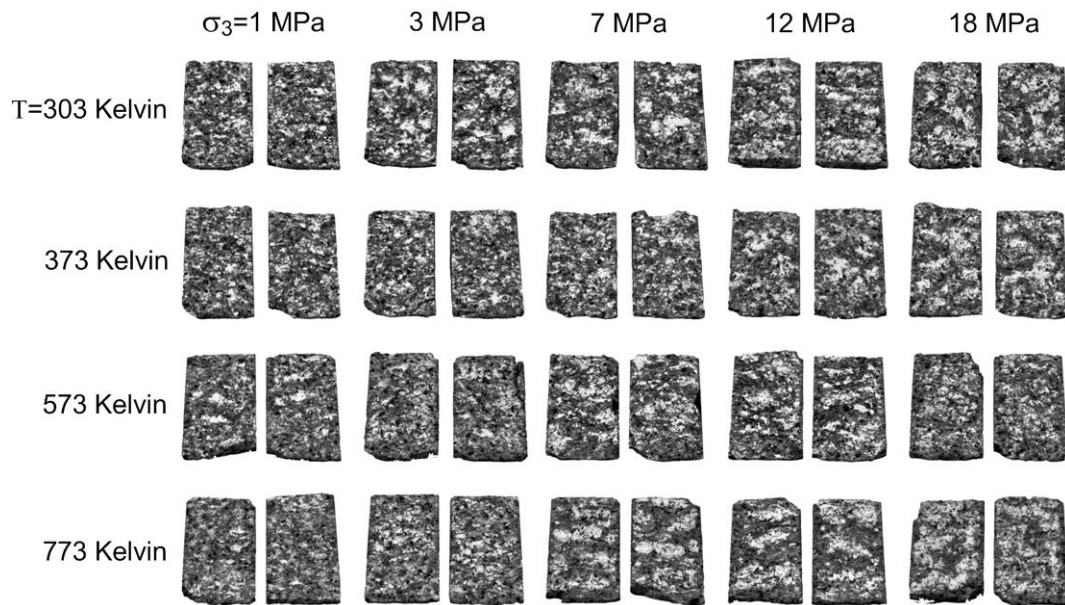
Figure 4.10 Post-test specimens from shear strength testing under different

confining pressures and temperatures.

4.5.2 Shear strength of saw-cut surfaces

The test method and strength calculation for the saw-cut surface testing

are identical to those of the tension-induced fractures. The temperatures ranging from

303, 373, 573 and 773 Kelvin and the confining stresses are maintained constant at 1,

3, 7, 12 and 18 MPa. Table 4.2 summarizes the strength results. The shear stress-

displacement curves for all specimens are shown in Figure 4.11. They are presented in

the form of τ-σ_n diagram in Figure 4.12. It is found that the increasing temperatures

can notably increase the shear strength. Post-test observations show that wear tracks

for the surfaces under higher temperatures tend to be longer than those tested under

lower temperatures (Figure 4.13).

Table 4.2 Peak shear strengths of saw-cut surfaces.

Temperatures, T (Kelvin)	Confining pressures, σ_3 (MPa)	Axial strengths, σ_1 (MPa)	Normal stresses, σ_n (MPa)	Shear strengths, τ (MPa)
303	1	6	2.25	2.16
	3	13.14	5.53	4.39
	7	24.29	11.32	7.49
	12	36.9	18.22	10.78
	18	52.87	26.72	15.1
373	1	6.19	2.3	2.25
	3	13.84	5.71	4.69
	7	21.56	10.64	6.3
	12	37.47	18.37	11.03
	18	54.71	27.18	15.89
573	1	8.88	2.97	3.41
	3	20.69	7.42	7.66
	7	28.5	12.38	9.31
	12	42.15	19.54	13.06
	18	55.43	27.36	16.21
773	1	19.59	5.65	8.05
	3	29.73	9.68	11.58
	7	37.38	14.59	13.15
	12	53.95	22.49	18.17
	18	66.99	30.24	21.21
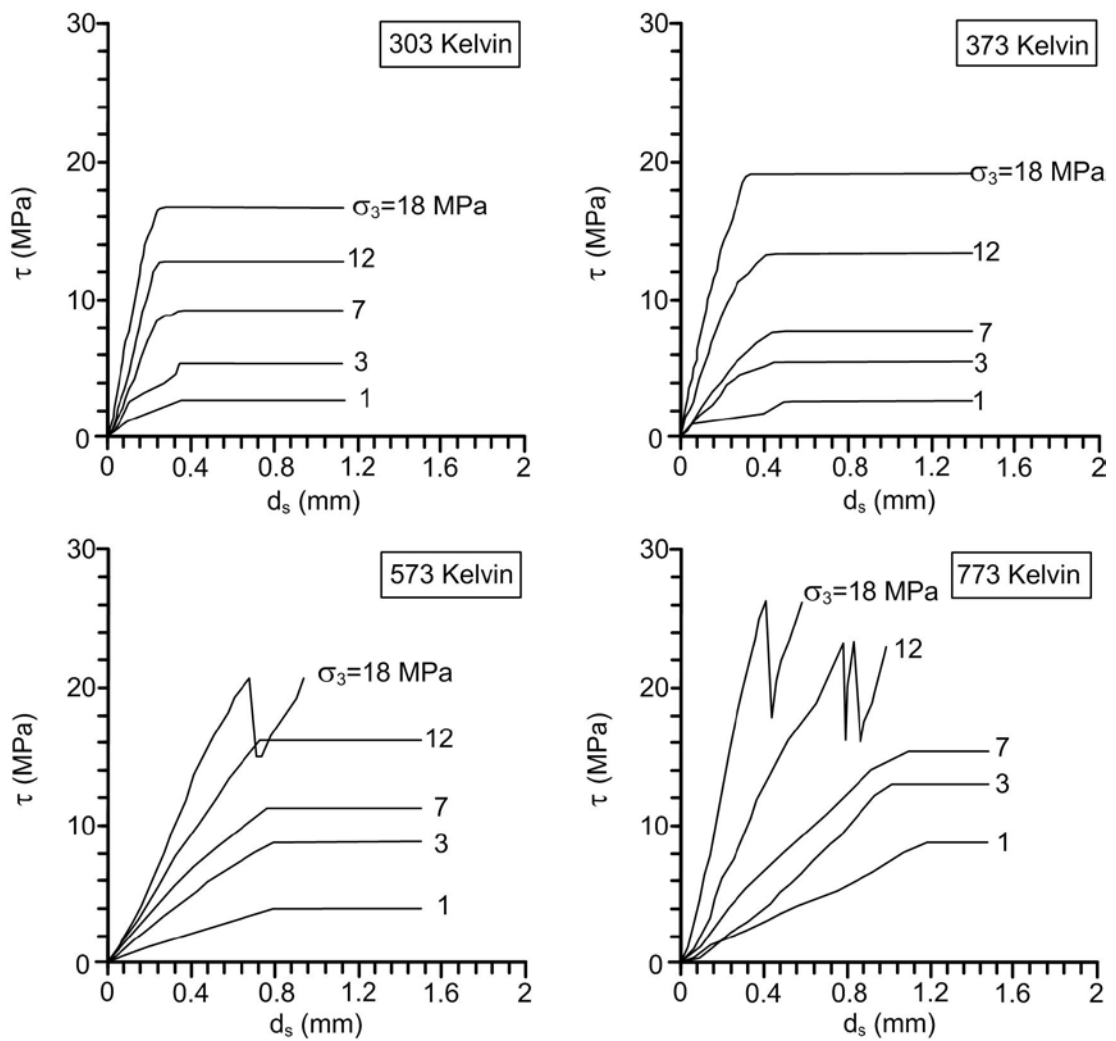
Figure 4.11 Shear stresses as a function of shear displacements of saw-cut surfaces.
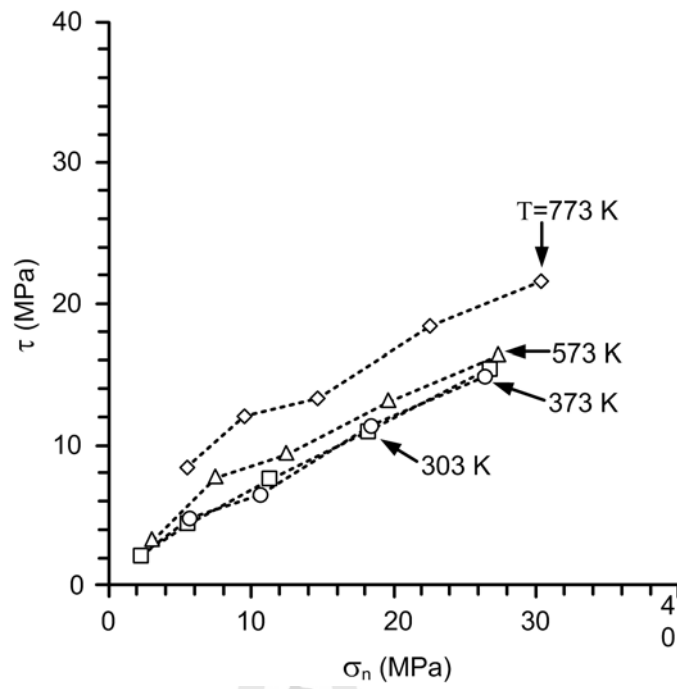
Figure 4.12 Shear stresses as a function of normal stresses of saw-cut surfaces.
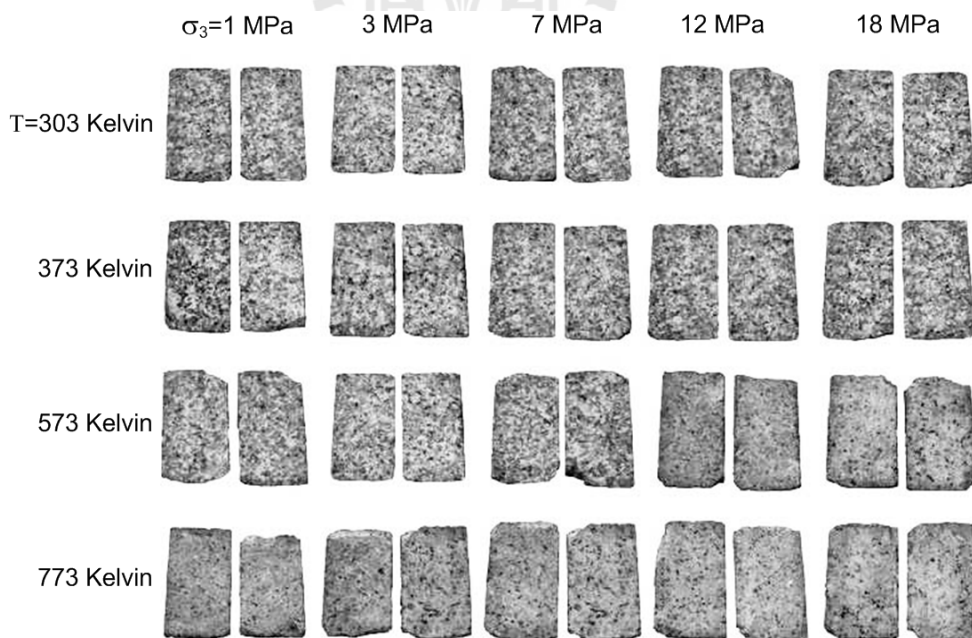
Figure 4.13 Post-test specimens from shear strength testing under different

confining pressures and temperatures.

CHAPTER V

MATHEMATICAL EQUATIONS

5.1   Introduction

The mathematical equations performed in this study aims at predicting the effects of temperatures on shear strength of rock fractures. The regression analysis is performed by using Barton's criterion (Barton and Choubey, 1977) for tension-induced fractures and empirical equation for saw-cut surfaces. The equation of tension-induced fracture is compared with Kirsch's solution.

5.2   Mathematical equation of tension-induced fractures

The results on tension-induced fractures indicate that the temperature can significantly reduce the fracture shear strengths. The non-linear behavior of the fracture is reflected as a curvature of shear strengths-normal stresses relation. Based on the Barton's criterion the peak shear strengths can be defined as:

$$\tau = \sigma_n \tan(\phi_b + JRC \, Log(\sigma_j/\sigma_n)) \tag{5.1}$$

where ϕ_b is basic friction angle of saw-cut surfaces, JRC is joint roughness coefficient, σ_j is joint wall compressive strength. Figure 5.1 compares the test data with the fitting curves of the Barton's criterion by regression analysis using SPSS statistical software (Wendai, 2000). Good coefficient of correlation between the

proposed equation and the test data is obtained (R^2=0.993). The relationship between

joint   wall   compressive

strength and elevated temperatures (Figure 5.2) can be represented by an exponential equation:

$$\sigma_j = \alpha \cdot \exp(\lambda \cdot T) \qquad (5.2)$$

where α and λ are empirical constants. T is absolute temperature. The parameters are defined by a regression analysis on the test data using SPSS statistical software as: $\alpha = 12000$, and $\lambda = -0.003$.

By substituting Equation (5.2) into (5.1) the following relation is obtained:

$$\tau = \sigma_n \tan(\phi_b + JRC \, Log(\alpha \cdot \exp(\lambda \cdot T)/\sigma_n) \qquad (5.3)$$

This equation can be used to predict shear strength of fractures in granite under elevated temperatures.

5.3 Mathematical equation of saw-cut surfaces

.   The test results are presented in the form of τ-σ_n diagram in Figure 4.5. It is found that the increasing temperatures can clearly increase the cohesion, which can be described by an empirical equation.

$$\tau = \xi \cdot \sigma_n + \chi \cdot \exp(\omega/T) \qquad (5.4)$$

where ξ, χ, ω are empirical constants. The parameters are defined by a regression analysis on the test data using SPSS statistical software as: $\xi = 0.54$, $\chi = 28.04$, and $\omega = -1300$. Good coefficient of correlation between the proposed equation and the test

data is obtained (R^2=0.983). Figure 5.3 compares the test data with the fitting curves

of the proposed equation. This equation can be used to predict shear strength of saw-

cut surface under elevated temperatures.
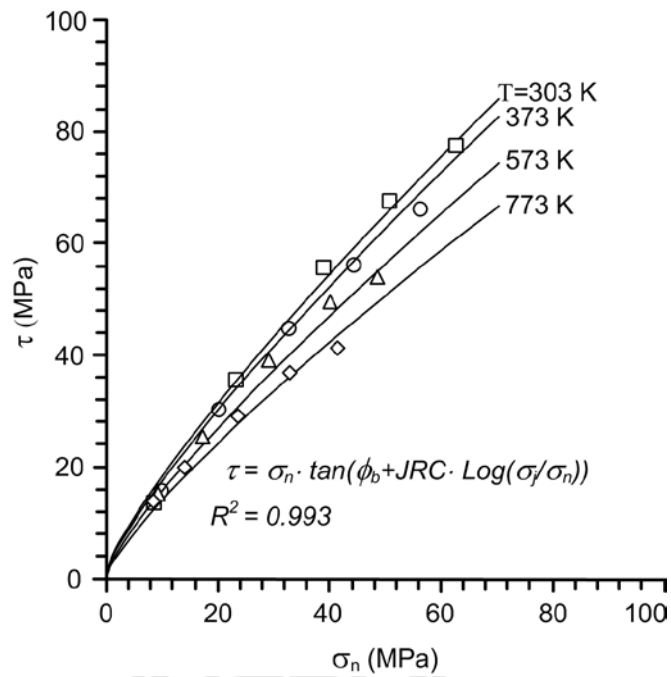
Figure 5.1   Comparison between tests result (points) and curves fit (lines) of

tension-induced fracture.

$$\sigma_J = 12000 \cdot exp(-0.003 \cdot T)$$
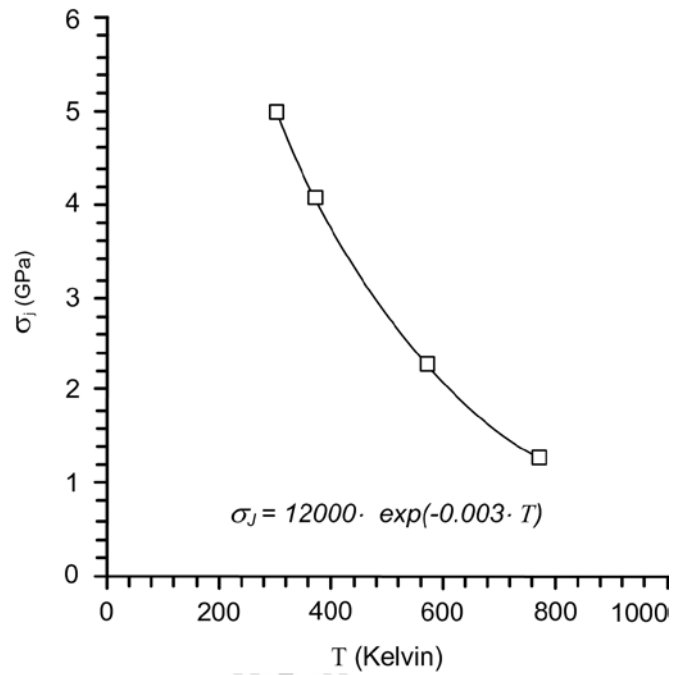
Figure 5.2 Relation between joint compressive strength (σ_j) and temperatures (T).

$$\tau = 0.54 \cdot \sigma_n + 28.04 \cdot exp(-1300/T)$$
$$(R^2 = 0.983)$$
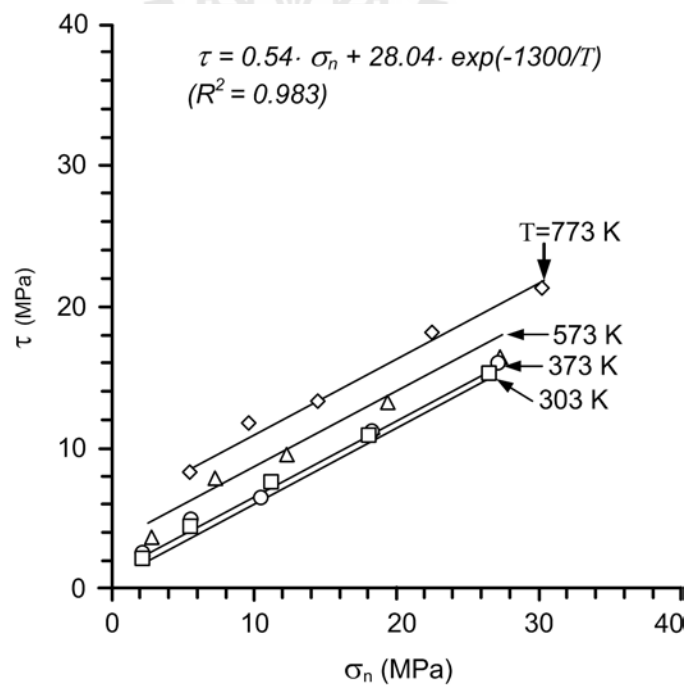
Figure 5.3 Comparison between tests result (points) and curves fit (lines) of saw-cut

surfaces.

5.4   Kirsch's solution

The kirsch equations are a set of closed-form solutions, derived from the theory of elastic, used to calculate the stress (Figure 5.4) and displacements around a circular excavation (Brady and Brown, 2006). The stress distributions around a borehole can be calculated by:

$$\sigma_r = \left[\frac{P_x + P_y}{2}\right]\left[1-\left(\frac{a^2}{r^2}\right)\right]+\left[\frac{P_x - P_y}{2}\right]\left[1-\left(\frac{4a^2}{r^2}\right)+\left(\frac{3a^4}{r^4}\right)\right]\cos2\theta \qquad (5.5)$$

$$\sigma_\theta = \left[\frac{P_x + P_y}{2}\right]\left[1+\left(\frac{a^2}{r^2}\right)\right]-\left[\frac{P_x - P_y}{2}\right]\left[1+\left(\frac{3a^4}{r^4}\right)\right]\cos2\theta \qquad (5.6)$$

$$\tau_{r\theta} = \left[\frac{P_y - P_x}{2}\right]\left[1+\left(\frac{2a^2}{r^2}\right)-\left(\frac{3a^4}{r^4}\right)\right]\sin2\theta \qquad (5.7)$$
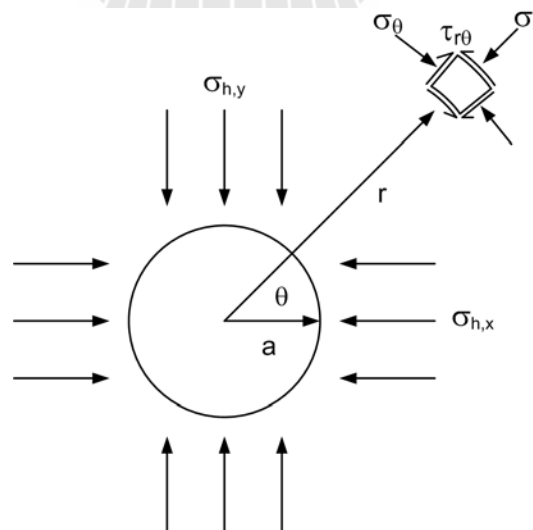
Figure 5.4   Stresses distribution around the borehole (Brady and Brown, 2006).

where σ_r is the stress in the direction of changing r, σ_θ is tangential stress, $\tau_{r\theta}$ is shear stress, P_y is vertical stress, P_x is lateral stress, a is inside radius of opening equal 3, r is variable radius and θ is the angle between vertical axis and radius.

The estimated in-situ stresses are proposed by Brady and Brown (2006) as;

$$\sigma_v = 0.027 \cdot z \tag{5.8}$$

$$\sigma_h = k \cdot \sigma_v \tag{5.9}$$

$$k = (1500/z) + 0.5 \tag{5.10}$$

where σ_v is vertical stress (MPa), σ_h is horizontal stress (MPa) and z is depth (m).

For a conservative design the shear stress around borehole define the relationship between the stress in direction y ($\sigma_{h,y}$) is three times the horizontal stress in direction x ($\sigma_{h,x}$).

5.5 Kirsch's solution results

The results from Kirsch equation are found that the maximum shear stress has angle of 45° and distance normalized of 1.73 (from borehole center of 5.2 m) shown in Figure 5.5. The maximum shear stresses around borehole obtained used here to calculate the factor of safety (FS) by comparing these with proposed equation (Equation 5.3).

The calculated factor of safety on tension-induced fractures and saw-cut surfaces are shown in Tables 5.1 and 5.2, respectively. The results indicate that the factors of safety of tension-induced fractures decrease with increasing temperatures.

These may can indicate that the joint roughness of the fractures have no effect to shear strength under extreme condition (the temperatures higher than tested here). Figure 5.6 shows the comparison between shear stress around borehole and shear strength from the mathematical equation both of tension-induced fractures and saw-cut-surfaces.
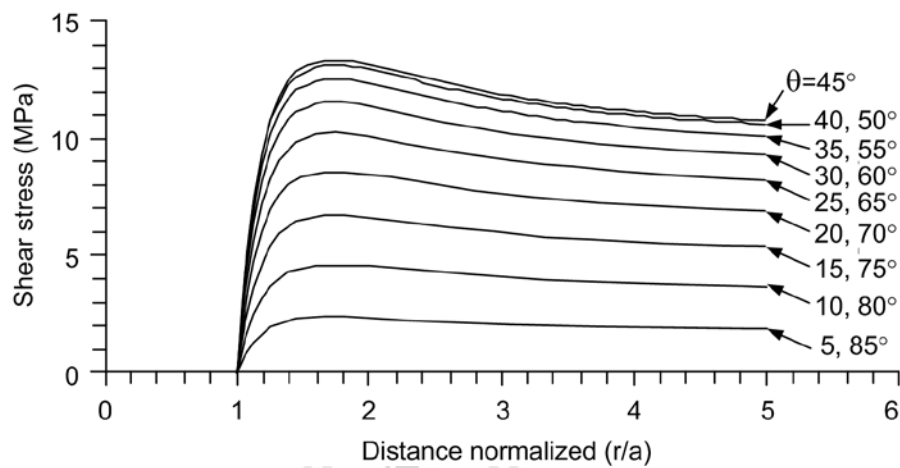
Figure 5.5 Shear stress as a function of distance normalized.
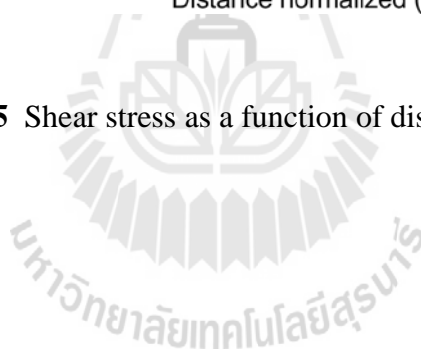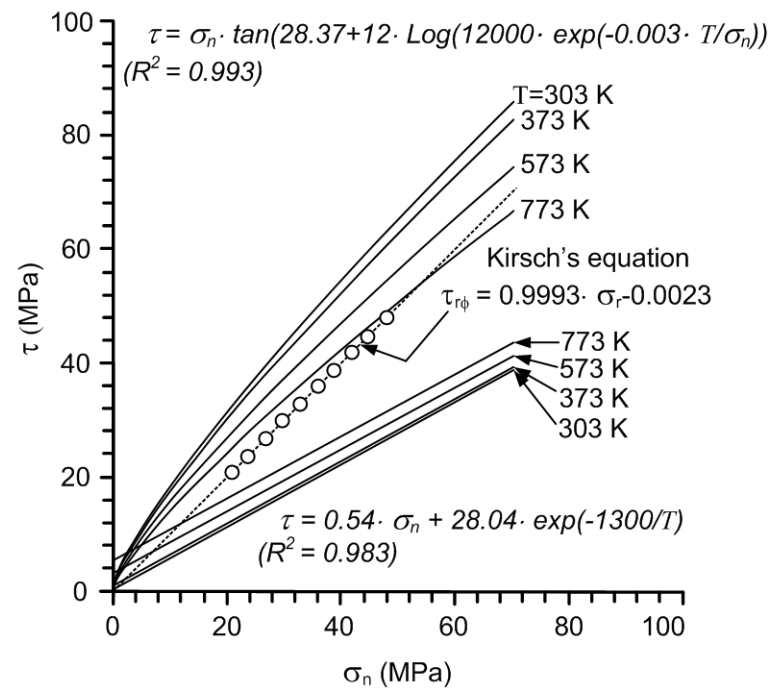
Figure 5.6 Comparison between shear stress from Kirsch's solution and from

mathematical equation.
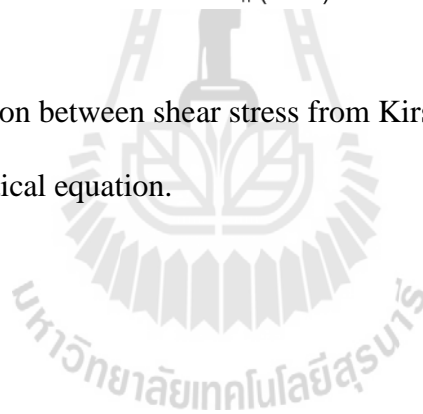
Table 5.1 Factors of safety of fracture around borehole (tension-induced fractures).

Depth, z (m)	σ_v (MPa)	k	$\sigma_{h,y}$ (MPa)	$\sigma_{h,x}$ (MPa)	σ_r, σ_n (MPa)	$\tau_{r\theta}$ (MPa)	Temperature at 303 Kelvin		Temperature at 773 Kelvin	
							τ (MPa)	Factor of Safety	τ (MPa)	Factor of Safety
500	13.50	3.5	47.25	15.75	21.02	21	32.01	1.52	24.49	1.17
1000	27.00	2.0	54.00	18.00	24.02	24	35.63	1.48	27.31	1.14
1500	40.50	1.5	60.75	20.25	27.02	27	39.17	1.45	30.06	1.11
2000	54.00	1.3	67.50	22.50	30.02	30	42.64	1.42	32.77	1.09
2500	67.50	1.1	74.25	24.75	33.02	33	46.05	1.40	35.42	1.07
3000	81.00	1.0	81.00	27.00	36.03	36	49.41	1.37	38.04	1.06
3500	94.50	0.9	87.75	29.25	39.03	39	52.72	1.35	40.61	1.04
4000	108.00	0.9	94.50	31.50	42.03	42	55.98	1.33	43.14	1.03
4500	121.50	0.8	101.25	33.75	45.03	45	59.20	1.32	45.65	1.01
5000	135.00	0.8	108.00	36.00	48.04	48	62.39	1.30	48.13	1.00
5500	148.50	0.8	114.75	38.25	51.05	51	65.55	1.29	50.58	0.99
6000	162.00	0.8	121.50	40.50	54.06	54	68.67	1.27	53.01	0.98

Table 5.2 Factors of safety of fracture around borehole (saw-cut surfaces).

Depth, z (m)	σ_v (MPa)	k	$\sigma_{h,y}$ (MPa)	$\sigma_{h,x}$ (MPa)	σ_r, σ_n (MPa)	$\tau_{r\theta}$ (MPa)	Temperature at 303 Kelvin		Temperature at 773 Kelvin	
							τ (MPa)	Factor of Safety	τ (MPa)	Factor of Safety
500	13.50	3.5	47.25	15.75	21.02	21	11.73	0.56	16.57	0.79
1000	27.00	2.0	54.00	18.00	24.02	24	13.35	0.56	18.19	0.76
1500	40.50	1.5	60.75	20.25	27.02	27	14.97	0.55	19.81	0.73
2000	54.00	1.3	67.50	22.50	30.02	30	16.59	0.55	21.43	0.71
2500	67.50	1.1	74.25	24.75	33.02	33	18.21	0.55	23.05	0.70
3000	81.00	1.0	81.00	27.00	36.03	36	19.84	0.55	24.67	0.69
3500	94.50	0.9	87.75	29.25	39.03	39	21.46	0.55	26.29	0.67
4000	108.00	0.9	94.50	31.50	42.03	42	23.08	0.55	27.91	0.66
4500	121.50	0.8	101.25	33.75	45.03	45	24.70	0.55	29.53	0.66
5000	135.00	0.8	108.00	36.00	48.04	48	26.33	0.55	31.16	0.65
5500	148.50	0.8	114.75	38.25	51.05	51	27.95	0.55	32.78	0.64
6000	162.00	0.8	121.50	40.50	54.06	54	29.58	0.55	34.41	0.64

CHAPTER VI

DISCUSSIONS AND CONCLUSIONS

6.1   Discussions and conclusions

The results of shear strength on rough fracture indicate that elevated temperatures effect to granite behavior. The effect of temperatures is insignificant below 573 kelvin, suggesting that this temperature ranges is in the brittle regime. Above 573 kelvin, the temperatures effect is greater (Ohnaka, 1995). The increasing temperatures are the cause of shear displacement increasing and shear strength decreasing. This may be related to development of localized plastic deformation in shear failure zone. The shear strength on saw-cut surface is increased by increasing temperatures. The result agrees with results obtained by Lockner et al. (1986) and Mitchell et al. (2013). This may be explained by that surface roughness of saw-cut surface is increased by increasing temperatures; therefor, the cohesion is increased (Parthasarathi et al., 2013). Stick-slip phenomenon is found at temperatures of 573 and 773 kelvin and confining pressures of 12 and 18 MPa. The post-test of saw-cut samples show the scratch on the surfaces. The scratching results in an increase in frictional resistance and impedes further sliding on the saw-cut surface at higher temperatures. Once sliding has stopped, shearing stress increases until the shear strength of the asperities is exceeded; besides, the stick-slip phenomenon depends on mineral composition (Kawamoto and Shimamoto 1998).

From the relationship between shear strength as a function of normal stresses under elevated temperatures of tension-induced fractures. This relationship can be described by the Barton's criterion. The shear strength of tension-induced fractures depends on joint wall compressive strengths under elevated temperatures. For the relationship between shear strength and normal stresses under elevated temperatures of saw-cut surfaces shows an opposite results compared to those of the tension-induced fractures. The SPSS regression analysis shows that the test data and empirical equation are agreeable. The fitting equation can be used to predict shear strength of fractures in granite around deep disposal borehole under the temperatures ranged here.

Comparison between the proposed equation and shear stress around borehole are shown by factors of safety value. It is found that the temperature affect to stability of fractures around borehole that the high temperature cause decrease on factor of safety of tension-induced fractures. The proposed equation is conservative for designing borehole. The shear strength on tension-induced is compared with saw-cut surfaces. The results indicate that the joint roughness of the fractures has no effect to shear strength under extreme condition.

6.2 Recommendations for future studies

The study in this research can be taken as a preliminary study. More laboratory testing should be performed using the higher temperatures with larger specimens. The effect of temperature should be considered on the true triaxial compressive test with a variety of rock fracture characteristics. The saw-cut surface is also important to further study the effect of healing time. Scratching on saw-cut

surface should be investigated by profilometer to further study the effect of stick-slip phenomena.

REFERENCES

Araújo, R. G. S., Sousa, J. L. A. O. and Bloch, M. (1997). Experimental investigation on the influence of temperature on the mechanical properties of reservoir rocks. **International Journal of Rock Mechanics and Mining Sciences** 34(3–4): 298.e1-298.e16.

Atherton, M., Brotherton, M., Mahawat, C. (1992). Integrated chemistry, textures, phase relations and modelling of a composite granodioritic-monzonitic batholith, Tak, Thailand. **Journal of Southeast Asian Earth Sciences** 7(2-3): 89-112.

Barton, N. (1982). Shear strength investigations for surface mining. In **Proceedings of the Third International Conference on Surface mining** (pp. 171-196). Vancouver.

Barton, N. R. and Choubey, V. (1977). The shear strength of rock joints in theory and practice. **Rock Mechanics** 10(1-2): 1-54.

Blanpied, M. L., Lockner, D. A. and Byerlee, J. D. (1995). Frictional slip of granite at hydrothermal conditions. **Journal of Geophysical** 100(B7): 13,045-13,064.

Brady, B. H. G. and Brown, E. T. (2006). **Rock Mechanics for Underground Mining** (pp 527). George Allen and Unwin, London.

Dwivedi, R. D., Goel, R. K., Prasad, V. V. R. and Sinha, A. (2008). Thermo-mechanical properties of Indian and other granites. **International Journal of Rock Mechanics and Mining Sciences** 45(3): 303-315.

Engelder J. T. (1976). Effect of scratch hardness on frictional wear and stick-slip of Westerly granite and Cheshire quartzite. In: **Strens RGI (ed) the physical and chemistry of minerals and rocks** (pp. 139-150)**.** April 1974, NATO Institute, Newcastle upon type, Wiley, London,.

Fuenkajorn, K. and Kenkhunthod, N. (2010). Influence of loading rate on deformability and compressive strength of three Thai sandstones. **Geotechnical and Geological Engineering** 28(5): 707-715.

Gibb, F. G. F (1999). High-temperature, very deep, geological disposal: a safer alternative for high-level radioactive waste? **Waste Management** 19(3): 207-211.

Gibb, F. G. F. (2003). Granite Recrystallization – The Key to an Alternative Strategy for HLW Disposal? In **Proceedings of the Twenty-seventh Material Research Society Symposium, Scientific Basis for Nuclear Waste Management** (vol. 807, pp. 937-942). Warrendale, Pa. MRS Online Proceedings Library.

Gibb, F. G. F., McTaggart, N. A., Travis, K. P., Burley, D. and Hesketh, K. W. (2008). High-density support maes: Key to the deep borehole disposal of spent nuclear fuel. **Journal of Nuclear Materials** 374(3): 370-377.

Gibb, F. G. F., Taylor, K. J. and Burakov, B. E. (2008). The 'granite encapsulation' route to the safe disposal of Pu and other actinides. **Journal of Nuclear Materials** 374(3): 364-369.

Hoek, E. and Brown, E. T. (1990). **Underground excavations in rock** (pp. 102-106). London. UK. Institution of Mining and Metallurgy.

Jaeger, J. C., Cook, N. G. W., Zimmerman, R. W. (2007). **Fundamentals of Rock Mechanics Fourth Edition** (pp 17-73). Blackwell Publishing, Oxford.

Kawamoto, E. and Shimamoto, T. (1998). The strength profile for bimineralic shear zones: an insight from high-temperature shearing experiments on calcite–halite mixtures. **Tectonophysics** 295(1–2): 1-14.

Lane, K. S. and Heck, W. J. (1964). Triaxial testing for strength of rock joints, In **Proceedings of the Sixth U.S. Symposium on Rock Mechanics (USRMS)** (pp. 98-108). October 28-30, Rolla, Missouri.

Lockner, D. A., Summers, R. and Byerlee, J. D. (1986). Effects of temperature and sliding rate on frictional strength of granite. **Pure and Applied Geophysics** 124(3).

Mahawat, C., Atherton, M. P. A. and Brotherton, M. S. (1990). The Tak Batholith, Thailand: the evolution of contrasting granite types and implications for tectonic setting. **Journal of Southeast Asian Earth Sciences** 4(1): (11-27).

Mitchell, E. K., Fialko, Y. and Brown, K. M. (2013). Temperature dependence of frictional healing of Westerly granite: Experimental observations and numerical simulations. **Geochemistry, Geophysics, Geosystems** 14: 567-582.

Odedra, A., Ohnaka, M., Mochizuki, H. and Sammonds, P. (2001). Temperature and pore pressure effects on the shear strength of granite in the brittle-plastic transition regime. **Geophysical Research Letters** 28(15): 3011-3014.

Ohnaka, M. (1995). A shear failure strength law of rock in the brittle-plastic transition regime. **Geophysical Research Letters** 22 (1): 25-28.

Parthasarathi, N. L., Borah, U. and Albert, S. K. (2013). Effect of temperature on sliding wear of AISI 316 L(N) stainless steel – Analysis of measured wear and surface roughness of wear tracks. **Materials & Design** 51: 676-682.

Rocscience Inc. (2012). **Examine^{2D} Version 8.0 - 2D Stress Analysis for Underground Excavations.** www.rocscience.com, Toronto, Ontario, Canada.

Rosso, R. S. (1976). A comparison of joint stiffness measurement in direct shear, triaxial compression and in situ. **International Journal of Rock Mechanics and Mining Sciences and Geomechanics Abstracts** 13(6): 167-172.

Stesky, R. M. (1975). The mechanical behaviour of faulted rock at high temperature and pressure. **Thesis doctor of Massachusetts Institute of Technology.**

Stesky, R. M. (1978). Rock Friction-Effect of Confining Pressure, Temperature, and Pore Pressure. **Pure and Applied Geophysics** 116.

Stesky, R. M., Brace, W. F., Riley, D. K. and Robin, P. Y. F. (1974). Friction in faulted rock at high temperature and pressure. **Tectonophysics** 23: 177-203.

Sundberg, J., Back, P. E., Christiansson, R., Hökmark, H., Ländell, M. and Wrafter, J. (2009) Modelling of thermal rock mass properties at the potential sites of a Swedish nuclear waste repository. **International Journal of Rock Mechanics and Mining Sciences**. 46(6): 1042-1054

Tisa, A. and Kovari, K. (1984). Continuous failure state direct shear tests. **Rock Mechanics and Rock Engineering** 17: 83-95.

Wai, R. S. and Lo, K. Y. (1982). Temperature effects on strength and deformation behaviour of rocks in Southern Ontario. **Canadian Geotechnical Journal** 19(3): 307-319

Wendai, L. (2000). Regression analysis, linear regression and probit regression In 13 chapters. **SPSS for windows: statistical analysis.** Publishing House of Electronics Industry. Beijing.

Witherspoon, P. A., Gale, J. E. and Cook, N. G. W. (1979). Investigations in granite at stripa, Sweden for nuclear waste storage. **Annual Meeting of the American Nuclear Society**. June 3-8, Atlanta, Georgia.

Xu, X., Ga, F., Shen, X. and Xie, H. (2008). Mechanical characteristics and microcosmic mechanisms of granite under temperature loads. **Journal of China University of Mining and Technology** 18(3): 413-417.

Xu, X., Kang, Z., Ming, j., Ge, W. and Jing, C. (2009). Research of microcosmic mechanism of brittle-plastic transition for granite under high temperature. **Procedia Earth and Planetary Science** 1(1): 432-437.

Zhao, Y., Wan, Z., Feng, Z., Yang, D., Zhang, Y. and Qu, F. (2012). Triaxial compression system for rock testing under high temperature and high pressure. **International Journal of Rock Mechanics and Mining Sciences** 52: 132-138.

BIOGRAPHY

Mr. Pakpoom Naphudsa was born on December 28, 1987 in Nakhon Ratchasima province, Thailand. He received his Bachelor's Degree in Engineering (Geotechnology) from Suranaree University of Technology in 2010. For his post-graduate, he study with a Master's degree in the Geological Engineering Program, Institute of Engineering, Suranaree university of Technology. During graduation, 2012-2013, he was a part time worker in position of research assistant at the Geomechanics Research Unit, Institute of Engineering, Suranaree University of Technology.